Combined analysis of Belle and Belle II data to determine the CKM angle ϕ_3 using $B^+ \to D(K_S^0 h^+ h^-) h^+$ decays

The Belle and Belle II collaborations

E-mail: niharikarout@physics.iitm.ac.in, coll-publications@belle2.org

ABSTRACT: We present a measurement of the Cabibbo-Kobayashi-Maskawa unitarity triangle angle ϕ_3 (also known as γ) using a model-independent Dalitz plot analysis of $B^+ \to D\left(K_S^0 h^+ h^-\right) h^+$, where D is either a D^0 or $\bar{D}^0$ meson and h is either a π or K. This is the first measurement that simultaneously uses Belle and Belle II data, combining samples corresponding to integrated luminosities of $711\,\text{fb}^{-1}$ and $128\,\text{fb}^{-1}$, respectively. All data were accumulated from energy-asymmetric e^+e^- collisions at a centre-of-mass energy corresponding to the mass of the $\Upsilon(4S)$ resonance. We measure $\phi_3 = (78.4 \pm 11.4 \pm 0.5 \pm 1.0)^\circ$, where the first uncertainty is statistical, the second is the experimental systematic uncertainty and the third is from the uncertainties on external measurements of the D-decay strong-phase parameters.

Contents

1 Introduction

The Cabibbo-Kobayashi-Maskawa (CKM) unitarity triangle describes CP violation within the Standard Model (SM) of particle physics. The sides and angles of the unitarity triangle are related to the elements of the CKM matrix [1, 2]. The angle ϕ_3, also known as γ, is defined as $\phi_3 \equiv \arg\left(-V_{ud}V^*_{ub}/V_{cd}V^*_{cb}\right)$, where $V_{qq'}$ are CKM matrix elements. The angle is measurable via the interference of the tree-level quark transitions $\bar{b} \to \bar{c}u\bar{s}$ and $\bar{b} \to \bar{u}c\bar{s}$,[1] which involve the emission of a W^+ boson from the $\bar{b}$ quark. The tree-level nature of these transitions results in negligible theoretical uncertainties when interpreting the measured observables in terms of ϕ_3 [3]. Therefore, assuming the absence of new physics at tree level, the measurement of ϕ_3 provides a test of the SM when compared to indirect determinations. The latter are derived from independent measurements of the sides and other angles of the unitarity triangle, which can be influenced by beyond-the-SM particles via loop amplitudes [4]. The world-average value of the direct measurements of ϕ_3 is $\left(66.2^{+3.4}_{-3.2}\right)^\circ$ [5].[2]

---

[1]Throughout this paper charge-conjugate processes are included unless explicitly stated otherwise.

[2]Updated results and plots available at https://hflav.web.cern.ch/.

The indirect determination of ϕ_3 is $(63.4 \pm 0.9)°$ [6]. Therefore, improvement in the direct determination of ϕ_3 is required to better constrain possible beyond-the-SM contributions to CP violation.

The world average is dominated by a result reported by the LHCb collaboration [7] that uses measurements of direct CP violation in the decays $B^+ \to D\left(K_S^0 h^+ h^-\right) h^+$, where D is either a D^0 or $\bar{D}^0$ and h is a pion or kaon [8–10]. The interference between $\bar{b} \to \bar{c}u\bar{s}$ and $\bar{b} \to \bar{u}c\bar{s}$ arises because the D^0 or $\bar{D}^0$ decay to the same $K_S^0 h^+ h^-$ final state. The $D \to K_S^0 h^+ h^-$ decays proceed via several intermediate resonances, which results in a variation of the CP asymmetry over phase space such that ϕ_3, as well as other parameters related to the B-decay amplitude, can be determined from a single decay. This property is in contrast to measurements of ϕ_3 that use $B^+ \to DK^+$ decays in which the D decays to a two-body final state, such as the CP-eigenstate $K_S^0\pi^0$ [11, 12] or $K^\pm\pi^\mp$ [13, 14].

Two approaches are used to determine ϕ_3 from $B^+ \to D\left(K_S^0 h^+ h^-\right) h^+$ decays, which are either dependent [8–10] or independent [8] of modelling the $D^0 \to K_S^0 h^+ h^-$ decay amplitude. The model-dependent method relies upon a detailed description of the intermediate-resonance structure of the D-decay amplitude. The model-independent method uses CP-asymmetry measurements in disjoint regions (bins) of the D-decay phase space that can then be related to ϕ_3 using measurements of D-decay strong-phase parameters determined by the CLEO [15] and BESIII [16, 17] collaborations. The loss of information that results from binning data in the model-independent method is compensated by the removal of potentially large and difficult-to-determine systematic uncertainties from the assumptions of the amplitude model, which are unavoidable in the model-dependent method. These model-dependent uncertainties have been estimated to be between 3° [18] to 9° [19]. Due to this systematic limitation, the world-leading measurement [7] and most other recent measurements, use the model-independent method.

In this paper we report a model-independent measurement of ϕ_3 using $B^+ \to D\left(K_S^0 h^+ h^-\right) h^+$ decays produced in asymmetric e^+e^- collisions at a centre-of-mass (c.m.) energy corresponding to the mass of the $\Upsilon(4S)$ resonance. The data sample used corresponds to integrated luminosities of $711\,\mathrm{fb}^{-1}$ and $128\,\mathrm{fb}^{-1}$ accumulated by the Belle and Belle II experiments, respectively. This result is the first obtained from a combined analysis of Belle and Belle II data. The results in this paper supersede a previous model-independent measurement using the full Belle data set [20]. The measurement presented here includes significant improvements compared to the earlier Belle measurement, which are related to background reduction, K_S^0 meson selection, reduced systematic uncertainties, and the addition of $D \to K_S^0 K^+ K^-$ decays.

The organisation of this paper is as follows. Section 2 presents an outline of the analysis, which includes the formalism related to the model-independent method. Section 3 describes the Belle and Belle II experiments. Section 4 introduces the data sets and simulation samples used to perform the measurements. Sections 5 and 6 contain descriptions of the $B^+ \to D\left(K_S^0 h^+ h^-\right) h^+$ candidate selection and CP-violating observable extraction, respectively. Section 7 describes the estimation of systematic uncertainties. Sections 8 and 9 present the results and conclusions, respectively.

2 Analysis overview and formalism

The analysis proceeds by selecting samples of $B^+ \to Dh^+$ decays in the Belle and Belle II data sets. The $B^+ \to D\pi^+$ decay is selected along with the $B^+ \to DK^+$ decay because it is a more abundant and topologically identical control sample. An unbinned maximum likelihood fit to the combined sample of $B^+ \to Dh^+$ candidates is used to determine CP-violating observables. In addition, nuisance parameters are determined, which limits dependence upon simulated data. The fit is to data categorised in several ways, including by the bin in which they are reconstructed in the D-decay Dalitz plot. To be model-independent, the fit relies upon the strong-phase parameters of the D decay measured in each of these bins, which are taken as external inputs. The CP-violating observables are then interpreted as constraints on ϕ_3 and hadronic parameters related to the B-decay amplitude. To avoid experimental bias analysis procedures are devised and validated on simulated samples before being applied to data. The remainder of this section describes the model-independent formalism used.

The two interfering decays sensitive to ϕ_3 are $B^+ \to \bar{D}^0 K^+$ and $B^+ \to D^0 K^+$, where the latter is both CKM- and colour-suppressed compared to the former. Thus, we write the total $B^+ \to D\left(K_S^0 h^+ h^-\right) K^+$, amplitude as

$$A_{B^+}\left(m_-^2, m_+^2\right) \propto A_{\bar{D}}\left(m_-^2, m_+^2\right) + r_B^{DK} e^{i\left(\delta_B^{DK} - \phi_3\right)} A_D\left(m_-^2, m_+^2\right), \qquad (2.1)$$

where $A_{\bar{D}}\left(m_-^2, m_+^2\right)$ $\left[A_D\left(m_-^2, m_+^2\right)\right]$ is the $\bar{D}^0 \to K_S^0 h^+ h^-$ $\left[D^0 \to K_S^0 h^+ h^-\right]$ decay amplitude at a point in the Dalitz plot described by m_-^2 and m_+^2, which are the squared invariant masses of the $K_S^0 h^-$ and $K_S^0 h^+$ particle combinations, respectively. Here r_B^{DK} and δ_B^{DK} are the ratio of the magnitudes of the suppressed to favoured $B^+ \to DK^+$ amplitudes and the relative strong-phase difference between them, respectively. The world-average value of r_B^{DK} is 0.0996 ± 0.0026 [5],[2] which means that the direct CP-violating effects are of the order 10%. The expression for the $B^- \to D\left(K_S^0 h^+ h^-\right) K^-$ amplitude A_{B^-} is obtained from eq. (2.1) by substituting $\phi_3 \to -\phi_3$ and $A_D\left(m_-^2, m_+^2\right) \longleftrightarrow A_{\bar{D}}\left(m_-^2, m_+^2\right)$. In this paper CP violation in D decays is considered to be negligible, such that $A_{\bar{D}}\left(m_-^2, m_+^2\right) = A_D\left(m_+^2, m_-^2\right)$.

In the model-independent method, the D-decay Dalitz plot is divided into $2 \times \mathcal{N}$ bins that are indexed from $i = -\mathcal{N}$ to $i = \mathcal{N}$, with $i = 0$ excluded. The bins are defined symmetrically about the line $m_+^2 = m_-^2$ such that if the point $\left(m_-^2, m_+^2\right)$ lies within bin i then point $\left(m_+^2, m_-^2\right)$ lies within bin $-i$; bins in which $m_-^2 > m_+^2$ are labelled with $i > 0$. The strong phase of the D^0-decay amplitude at a point $\left(m_-^2, m_+^2\right)$ is written as $\delta_D\left(m_-^2, m_+^2\right)$, from which the D-amplitude-weighted average of the cosine of the strong-phase difference between D^0 and $\bar{D}^0$ decays within bin i is defined as [8]

$$c_i = \frac{\int_i dm_-^2\, dm_+^2\, \left|A_D\left(m_-^2, m_+^2\right)\right| \left|A_D\left(m_+^2, m_-^2\right)\right| \cos\left[\delta_D\left(m_-^2, m_+^2\right) - \delta_D\left(m_+^2, m_-^2\right)\right]}{\sqrt{\int_i dm_-^2\, dm_+^2\, \left|A_D\left(m_-^2, m_+^2\right)\right|^2 \int_i dm_-^2\, dm_+^2\, \left|A_D\left(m_+^2, m_-^2\right)\right|^2}}, \quad (2.2)$$

where the integral is over the i-th bin. The D-amplitude-weighted average of the sine of the strong-phase difference within a bin s_i is defined in an analogous manner. These definitions result in the conditions $c_i = c_{-i}$ and $s_i = -s_{-i}$. Further, the A_{B^+} (A_{B^-}) amplitudes can

be squared and integrated over each bin to give the expectation for the B^+ (B^-) yields in each bin N_i^+ $\left(N_i^-\right)$,

$$N_i^+ = h_{B^+} \left[F_{-i} + \left\{ \left(x_+^{DK}\right)^2 + \left(y_+^{DK}\right)^2 \right\} F_i \quad + 2\sqrt{F_i F_{-i}} \left(x_+^{DK} c_i - y_+^{DK} s_i\right) \right],$$

$$N_{-i}^+ = h_{B^+} \left[F_i \quad + \left\{ \left(x_+^{DK}\right)^2 + \left(y_+^{DK}\right)^2 \right\} F_{-i} + 2\sqrt{F_i F_{-i}} \left(x_+^{DK} c_i + y_+^{DK} s_i\right) \right],$$

$$N_i^- = h_{B^-} \left[F_i \quad + \left\{ \left(x_-^{DK}\right)^2 + \left(y_-^{DK}\right)^2 \right\} F_{-i} + 2\sqrt{F_i F_{-i}} \left(x_-^{DK} c_i + y_-^{DK} s_i\right) \right],$$

$$N_{-i}^- = h_{B^-} \left[F_{-i} + \left\{ \left(x_-^{DK}\right)^2 + \left(y_-^{DK}\right)^2 \right\} F_i \quad + 2\sqrt{F_i F_{-i}} \left(x_-^{DK} c_i - y_-^{DK} s_i\right) \right], \quad (2.3)$$

where $h_{B^\pm}$ are independent normalisation constants, $x_\pm^{DK} = r_B^{DK} \cos\left(\delta_B^{DK} \pm \phi_3\right)$, and $y_\pm^{DK} = r_B^{DK} \sin\left(\delta_B^{DK} \pm \phi_3\right)$.[3] Here F_i is the fractional yield in each bin for a pure sample of D^0 decays accounting for any experiment-specific efficiency variation over the Dalitz plot [21]:

$$F_i = \frac{\int_i dm_-^2 \, dm_+^2 \, \left|A_D\left(m_-^2, m_+^2\right)\right|^2 \eta\left(m_-^2, m_+^2\right)}{\sum_j \int_j dm_-^2 \, dm_+^2 \, \left|A_D\left(m_-^2, m_+^2\right)\right|^2 \eta\left(m_-^2, m_+^2\right)}, \quad (2.4)$$

where the sum in the denominator is over all $2\mathcal{N}$ bins and $\eta\left(m_-^2, m_+^2\right)$ is the acceptance profile over the Dalitz plot, which depends on both laboratory-frame decay kinematics and the experimental setup.

The $4\mathcal{N}$ observables defined in eqs. (2.3) depend upon $4\mathcal{N}+4$ parameters: ϕ_3, r_B^{DK}, δ_B^{DK}, c_i, s_i, F_i and $h_{B^\pm}$. Therefore, independent measurements of the $2\mathcal{N}$ strong-phase parameters c_i and s_i are used to determine the other parameters from these yields. Furthermore, the $2\mathcal{N} - 1$ fractional yields F_i can be constrained using the simultaneous analysis of $B^+ \to D\pi^+$ decays [7], which have a branching fraction an order of magnitude larger than $B^+ \to DK^+$ [22]. An analogous set of yields for $B^+ \to D\pi^+$ exist as those defined in eq. (2.3), which depend upon $x_\pm^{D\pi} = r_B^{D\pi} \cos\left(\delta_B^{D\pi} \pm \phi_3\right)$ and $y_\pm^{D\pi} = r_B^{D\pi} \sin\left(\delta_B^{D\pi} \pm \phi_3\right)$, where $r_B^{D\pi}$ and $\delta_B^{D\pi}$ are the magnitude ratio and strong-phase difference between the Cabibbo- and colour-suppressed $B^+ \to D^0\pi^+$ amplitude and the favoured $B^+ \to \bar{D}^0\pi^+$ amplitude. The value of $r_B^{D\pi}$ is approximately 20 times smaller[4] than r_B^{DK} so the sensitivity to CP violation is significantly reduced in comparison to that from $B^+ \to DK^+$ decays. Given the almost identical kinematic properties between $B^+ \to DK^+$ and $B^+ \to D\pi^+$, the F_i parameters are common for the two sets of yields within a single experiment. We adopt a parameterisation [23, 24] that utilises the common dependence on ϕ_3 of the $B^+ \to DK^+$ and $B^+ \to D\pi^+$ yields by introducing the single complex variable,

$$\xi^{D\pi} = \left(\frac{r_B^{D\pi}}{r_B^{DK}}\right) e^{i\left(\delta_B^{D\pi} - \delta_B^{DK}\right)}. \quad (2.5)$$

---

[3] CP violation in the total decay rate is negligible, i.e., when integrated over the full Dalitz plot [7]. Therefore, to avoid any bias due to detector asymmetry, independent normalisation constants are used for B^+ and B^- decays.

[4] This factor is $\tan^2\theta_C$, where θ_C is the Cabibbo angle, which is the relative Cabibbo suppression of $r_B^{D\pi}$ with respect to r_B^{DK}.
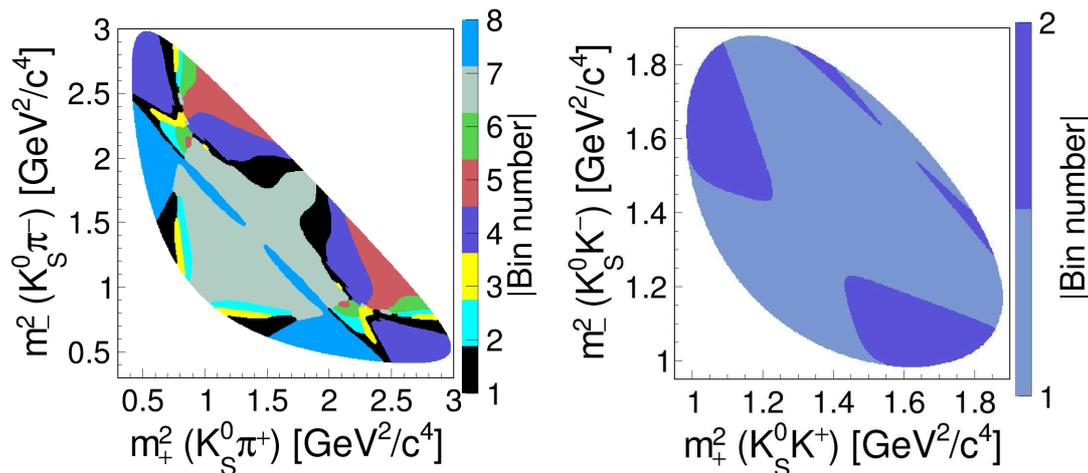
Figure 1. Binning schemes used for (left) $B^+ \to D\left(K_S^0\pi^+\pi^-\right)K^+$ decays and (right) $B^+ \to D\left(K_S^0 K^+ K^-\right)K^+$ decays.

Defining $x_\xi^{D\pi} \equiv \mathrm{Re}\left(\xi^{D\pi}\right)$ and $y_\xi^{D\pi} \equiv \mathrm{Im}\left(\xi^{D\pi}\right)$ we can write

$$x_\pm^{D\pi} = x_\xi^{D\pi}x_\pm^{DK} - y_\xi^{D\pi}y_\pm^{DK}, \quad y_\pm^{D\pi} = x_\xi^{D\pi}y_\pm^{DK} + y_\xi^{D\pi}x_\pm^{DK}. \tag{2.6}$$

The values of $x_\pm^{DK}$, $y_\pm^{DK}$, $x_\xi^{D\pi}$, $y_\xi^{D\pi}$ and F_i are determined simultaneously from a fit to the $B^+ \to Dh^+$ candidates. The advantages of this parameterisation are the inclusion of the ϕ_3 sensitivity from $B^+ \to D\pi^+$ in the determination of $x_\pm^{DK}$ and $y_\pm^{DK}$ as well as much improved fit stability [7]. Further, the determination of F_i by simultaneously fitting $B^+ \to Dh^+$ removes a source of systematic uncertainty in this analysis compared to that reported in ref. [20]. The previous Belle analysis [20] determined the values of F_i from a sample of $D^{*+} \to D^0\pi^+$ decays. The differing kinematic properties of the $B^+ \to D\pi^+$ and $D^{*+} \to D^0\pi^+$ decays resulted in different $\eta\left(m_-^2, m_+^2\right)$ acceptance functions for the two samples, which was a source of systematic uncertainty.

There are three binning schemes, for both $D^0 \to K_S^0\pi^+\pi^-$ and $D^0 \to K_S^0 K^+ K^-$ decays, for which c_i and s_i have been measured [16, 17]. We adopt the $\mathcal{N} = 8$ optimal binning for $B^+ \to D\left(K_S^0\pi^+\pi^-\right)h^+$ decays, which has been shown to have approximately 90% of the statistical sensitivity of an unbinned analysis [15, 25]. We adopt the $\mathcal{N} = 2$ equal-strong-phase binning for $B^+ \to D\left(K_S^0 K^+ K^-\right)h^+$ decays, which has better fit stability than the $\mathcal{N} = 3$ and 4 schemes [17] given the limited size of $B^+ \to D\left(K_S^0 K^+ K^-\right)K^+$ event sample. Figure 1 shows the two binning schemes used. The measurements of c_i and s_i ignore the effects of D-mixing and assume CP-conservation in D decay. Ignoring both these effects in the strong-phase and model-independent $B^+ \to D\left(K_S^0 h^+ h^-\right)h^+$ analyses, as in this paper, results in negligible bias [26]. The potential bias of ignoring K^0 CP-violation and regeneration has also been extensively studied [27] and a bias of $(0.4 \pm 0.1)^\circ$ on ϕ_3 is reported. This bias is negligible in comparison to the current statistical precision and is not considered further.

3 Belle and Belle II detectors

The Belle detector [28, 29] was located at the interaction point (IP) of the KEKB asymmetric-energy e^+e^- collider [30, 31]. The energies of the electron and positron beams were 8.0 GeV and 3.5 GeV, respectively. The detector subsystems most relevant for this study are the following: the silicon vertex detector and central drift chamber (CDC), for charged particle tracking and measurement of energy loss due to ionisation, and the aerogel threshold Cherenkov counters and time-of-flight scintillation counters, for particle identification (PID). These subsystems were situated in a magnetic field of 1.5 T. More detailed descriptions of the Belle detector can be found in refs. [28, 29].

The Belle II detector [32] is located at the IP of the SuperKEKB asymmetric-energy e^+e^- collider [33]. The energies of the electron and positron beams are 7.0 GeV and 4.0 GeV, respectively. The target instantaneous luminosity of SuperKEKB is a factor of 30 greater than KEKB, which will lead to significantly larger beam-related backgrounds. Therefore, the Belle II detector is an upgraded version of the Belle detector that is designed to cope with increased level of background. The detector contains several completely new subsystems, as well as substantial upgrades to others. The innermost subdetector is the vertex detector (VXD), which uses position-sensitive silicon sensors to precisely sample the trajectories of charged particles (tracks) in the vicinity of the IP. The VXD includes two inner layers of pixel sensors and four outer layers of double-sided silicon microstrip sensors. The second pixel layer is currently incomplete covering only one sixth of the azimuthal angle. Charged-particle momenta and charges are measured by a new large-radius, helium-ethane, small-cell CDC, which also offers charged-particle-identification information through a measurement of specific ionisation. The Belle PID system has been replaced. A Cherenkov-light angle and time-of-propagation (TOP) detector surrounding the CDC provides charged-particle identification in the central detector volume, supplemented by proximity-focusing, aerogel, ring-imaging Cherenkov (ARICH) detectors in the forward region with respect to the electron beam. The Belle CsI(Tl) crystal electromagnetic calorimeter, the Belle solenoid and iron flux return are reused in the Belle II detector. The electromagnetic calorimeter readout electronics have been upgraded and the instrumentation in the flux return to identify K_L^0 mesons and muons has been replaced.

4 Data sets

The analysis uses e^+e^- collision data collected at a c.m. energy corresponding to the mass of the $\Upsilon(4S)$ resonance. The integrated luminosities of the samples collected by Belle and Belle II are 711 fb^{-1} and 128 fb^{-1}, respectively.

Simulation samples are used to optimise the selection criteria, estimate signal efficiencies, train multivariate discriminants, identify various sources of background and develop a model to fit data. The signal and $e^+e^- \to \Upsilon(4S) \to B\bar{B}$ simulation samples are generated using the EVTGEN software package [34]. Samples of signal events are generated with the D-decay products following both resonant and non-resonant distributions. The Belle simulation samples of continuum background events $e^+e^- \to q\bar{q}$, where $q = u, d, s, c$, are generated by

PYTHIA [36]. The Belle II $e^+e^- \to q\bar{q}$ simulation sample is generated using the KKMC [35] generator interfaced with PYTHIA. The EVTGEN package also simulates the decay of short-lived particles. The Belle (Belle II) simulation samples use a GEANT3-based simulation package [37] (GEANT4 [38]) to model the detector response to the final-state particles. Final-state radiation effects are taken into account by including the PHOTOS model [39]. Belle simulation includes the effect of beam background by overlaying data taken that is unrelated to e^+e^- collisions (random triggers). Belle II simulation samples include the effect of simulated beam-induced background caused by the Touschek effect (scattering and loss of beam particles) and by beam-gas scattering, as well as luminosity-dependent backgrounds caused by Bhabha scattering and two-photon quantum electrodynamic processes [40].

5   Reconstruction and event selection

We use the Belle II analysis software framework (basf2) [41] for decay-chain reconstruction. The Belle II data are processed using this framework, whereas the tracks and clusters in the processed Belle data are converted to basf2 format using the B2BII software package [42]. Hence, the reconstruction software is identical for both the data samples.

The selections are similar to those described in ref. [20]. We apply nearly identical event selection criteria, with some slight differences due to the different detector configurations.

An overview of the selection procedure is as follows. We reconstruct the decay mode $B^+ \to D\left(K_S^0 h^+ h^-\right) h^+$. We select the π^+ and K^+ candidate tracks, as well as K_S^0 candidates, with selections designed to maximise the product of efficiency and purity. From these samples, $D \to K_S^0 h^+ h^-$ candidates are reconstructed, which are further combined with an h^+ track to form a B^+ candidate. Vertex and kinematic fits are performed, which constrain the B-decay products to a common vertex. Additional criteria are developed to suppress background events. The remainder of this section describes the motivation for the various selection requirements.

Charged particles, π^+ and K^+, consistent with originating from e^+e^- collisions are selected by requiring the distance of closest approach to the IP to be less than $0.2\,\mathrm{cm}$ in the plane transverse to and $1.0\,\mathrm{cm}$ along the z direction; in both the Belle and Belle II coordinate system the z-axis is defined to lie along the axis of symmetry of the solenoid approximately in the direction of the e^- beam. These charged particles are then identified as either kaons or pions by using the information from the CDC, the aerogel threshold Cherenkov counters and time-of-flight scintillation counters of Belle, and all subdetectors of Belle II, though that from CDC, TOP and ARICH is most significant. To identify kaon and pion candidates, we use the ratio $\mathcal{R}_{K/\pi} = \mathcal{L}(K)/\left[\mathcal{L}(K) + \mathcal{L}(\pi)\right]$, where $\mathcal{L}(h)$ is the likelihood for the particle h to produce the observed particle-identification signal associated with the track. We use a requirement of $\mathcal{L}(K/\pi) > 0.6$ to separate the kaons from pions coming directly from the $B^+ \to Dh^+$ decays. The kaon-identification efficiency is 84% (79%) and the probability of a pion being misidentified as a kaon is 8% (7%) in Belle [43] (Belle II) data. A less restrictive requirement of $\mathcal{L}(K/\pi) > 0.2$ is applied to the kaons used to reconstruct the $D \to K_S^0 K^+ K^-$ candidates, which suppresses the K-π misidentification rate while maintaining high efficiency. For Belle II data, there is an

additional requirement of $\cos\theta > -0.6$, where θ is the polar angle in the laboratory frame, applied to the π or K candidates that come directly from the B meson decays. This criterion removes the tracks outside the acceptance region of the TOP and ARICH, which reduces the K-π misidentification rate. Furthermore, this requirement increases the separation of the contribution from misidentified $B^+ \to D\pi^+$ decays from that of correctly reconstructed $B^+ \to DK^+$ decays [44]. We do not apply this selection to the Belle data because the contribution to the misidentified $B^+ \to D\pi^+$ decays is much smaller in this region, due to fewer tracks having $\cos\theta < -0.6$ as a result of the higher c.m. boost of the KEKB collider

Candidate K_S^0 mesons are reconstructed from pairs of oppositely charged particles, selected assigning the pion-mass hypothesis, that originate from a common vertex. The K_S^0 candidates are required to have an invariant mass in the interval $0.487 - 0.508\,\mathrm{GeV}/c^2$, which corresponds to $\pm 3\sigma$ around the known K_S^0 mass [22]. Here σ is the invariant mass resolution. A multivariate technique is used to improve the purity of the K_S^0 candidate sample by rejecting combinatorial background. Algorithms based on a neural network (NN) [45] and a fast boosted decision tree (FastBDT) [46] are used to identify the background in Belle and Belle II data, respectively. Five input variables are common to the Belle and Belle II algorithms: the angle between the momentum vector and the vector between the IP and the decay vertex of the K_S^0 candidate, the longer and shorter distances of closest approach between the extrapolated tracks of the pion candidates and the IP, the flight distance of the K_S^0 candidate projected on to the plane transverse to the z axis, and the difference between the observed and known K_S^0 mass divided by the uncertainty in the observed mass. The following seven additional variables are input to the Belle NN discriminator: K_S^0 momentum in the lab frame, shortest distance between the two track helices projected along the z axis, the angle between pion momentum in the K_S^0 rest frame and the boost direction between the laboratory frame and the K_S^0 rest frame, and the number (presence) of CDC (silicon vertex detector) hits for each pion track. The efficiency and purity of the K_S^0 selection are 87% (91%) and 99% (97%), respectively, for Belle (Belle II). Here we define efficiency as the fraction of correctly reconstructed K_S^0 candidates retained by the classifier and the purity as the fraction of correctly reconstructed K_S^0 candidates in the selected sample. The values of efficiency and purity are determined from simulation samples. Achieving a similar performance in the product of efficiency and purity in Belle II and Belle motivates the reduced set of input variables; fewer input variables makes the algorithm more robust against any disagreements between data and simulation distributions. A kinematic-constrained fit is performed on selected candidates by restricting the reconstructed $\pi^+\pi^-$ mass to the known K_S^0 mass [22] to improve the four-momentum resolution.

The $D \to K_S^0\pi^+\pi^-$ ($D \to K_S^0K^+K^-$) meson candidates are reconstructed from a pair of oppositely charged pion (kaon) tracks and a K_S^0 candidate. The invariant mass of the D-decay products $m\left(K_S^0h^-h^+\right)$ is required to be in the range $1.85 - 1.88\,\mathrm{GeV}/c^2$. This interval corresponds to $\pm 3\sigma$ around the nominal D mass, where σ is the $m\left(K_S^0h^-h^+\right)$ resolution. A kinematic-constrained fit is performed by restricting the reconstructed mass to the known D^0 mass [22] to improve the four-momentum resolution. After the kinematic constraint some candidates have values of $\left(m_+^2, m_-^2\right)$ that lie outside the kinematic boundary of the $D \to K_S^0h^+h^-$ Dalitz plot. These candidates are not considered further because they

cannot be unambiguously associated with a Dalitz plot bin. Studies of simulated signal samples indicate this requirement reduces the signal selection efficiency by 0.3%.

A charged particle is combined with these D candidates to form a $B^+ \to Dh^+$ candidate. The kinematic variables used to separate signal B candidates are the beam-energy-constrained mass

$$m_{\text{bc}} = c^{-2} \sqrt{E_{\text{beam}}^{*2} - \left| \sum_i \vec{\mathbf{p}}_i^* \right|^2 c^2}, \tag{5.1}$$

and the beam-energy difference,

$$\Delta E = \sum_i E_i^* - E_{\text{beam}}^*, \tag{5.2}$$

where E_{beam}^* is the beam energy in the c.m. frame and E_i^* ($\vec{\mathbf{p}}_i^*$) is the energy (momentum) of the i-th B-decay product in the c.m. frame. The candidates are selected in the range $m_{\text{bc}} > 5.27 \, \text{GeV}/c^2$ and $-0.13 < \Delta E < 0.18 \, \text{GeV}$. In subsequent analysis, ΔE is used as a fit variable. Generally, partially reconstructed $B^+ \to D^{(*)} K^{(*)+}$ decays peak at lower ΔE values and are difficult to model. An asymmetric ΔE window is chosen to exclude these peaking structures from the analysis.

The dominant background comes from $e^+ e^- \to q\bar{q}$ events, which are suppressed by using the difference in topology with respect to $e^+ e^- \to \Upsilon(4S) \to B\bar{B}$ decays. The $q\bar{q}$ events have particle momentum spatially correlated in two directions, forming jet-like structures. In contrast, the particles from a $B\bar{B}$ event are distributed uniformly over the 4π solid angle in the c.m. frame because the B mesons do not have significant momentum. Separate FastBDT classifiers are applied to Belle and Belle II data because of the differing c.m. boost. The classifiers are trained using simulated samples with several discriminating observables related to both the whole event and signal-only angular configurations as input variables. We use five variables:

- a likelihood ratio obtained from a Fisher discriminant formed from the modified Fox-Wolfram moments [47, 48];

- the absolute value of the cosine of the angle between the signal-B-candidate momentum and the z direction in the $e^+ e^-$ c.m. frame;

- the cosine of the angle between the thrust axis of the signal B candidate and the thrust axis of the rest-of-the-event (ROE);[5]

- the distance between the position of the signal B-decay vertex and the vertex of the ROE along the z direction; and

- the B meson flavour-tagger output [49, 50].[6]

---

[5] The thrust axis for a collection of particle momenta is the direction along which the sum of the momenta is maximised. The rest-of-the-event refers to all measured tracks and clusters that are not used to reconstruct the signal.

[6] Reference [50] describes two Belle II flavour-tagging algorithms that have similar performance; we use the output of the category-based algorithm.

Decay mode	Efficiency (%)	
	Belle	Belle II
$B^+ \to D(K_S^0 \pi\pi)\pi^+$	21.77 ± 0.03	22.13 ± 0.05
$B^+ \to D(K_S^0 \pi\pi)K^+$	19.11 ± 0.03	19.79 ± 0.05
$B^+ \to D(K_S^0 KK)\pi^+$	16.26 ± 0.03	18.16 ± 0.05
$B^+ \to D(K_S^0 KK)K^+$	14.29 ± 0.03	16.73 ± 0.05

Table 1. $B^+ \to D\left(K_S^0 h^+ h^-\right) h^+$ signal efficiencies estimated from simulated non-resonant signal samples. The uncertainties are statistical only.

These variables do not have any significant correlation with the signal extraction variable ΔE. The FastBDT classifier output (C) distribution ranges from zero, where background events peak, to one, where the signal events peak. The signal extraction fit is to the two-dimensional distributions of ΔE and a transformed variable derived from C (C'), which is defined in section 6. We require $C > 0.15$ $(C > 0.2)$, which rejects 67% of the $q\bar{q}$ background with only 4% signal loss when applied to the Belle (Belle II) data set; this requirement allows a simpler modelling of the C' distribution in the fit with negligible loss of statistical precision. The $e^+ e^- \to c\bar{c}$ background is further suppressed by vetoing candidates arising from $D^{*+} \to D^0 \pi^+$ decays. We veto events in the range $0.143 < \Delta m < 0.148 \,\mathrm{GeV}/c^2$, where Δm is the mass difference between D^* and D candidates. This requirement rejects approximately 9% of the remaining background after all other criteria are applied.

The possibility of additional peaking background from charmless B decays is studied by performing the analysis on the sidebands of the $m\left(K_S^0 h^+ h^-\right)$ distributions. Candidates are selected from the sideband without any kinematic constraint to the D mass applied; the value of $m\left(K_S^0 h^+ h^-\right)$ of selected sideband candidates is constrained to that of the midpoint of the sideband for subsequent analysis, such that they are treated in an identical manner to those in the $m\left(K_S^0 h^+ h^-\right)$ signal region. Studies of the simulated samples indicate that contributions arise from $B^+ \to K^{*+} \pi^- \pi^+$, $B^+ \to K^{*+} \rho^0$ and $B^+ \to K^{*+} J/\psi$ decays. The yields are obtained from fits to sideband data following the procedure described in section 6. The expected yields of charmless background are found to be negligible compared to that of the signal. Therefore, the charmless background is not considered further in subsequent analysis, apart from as a source of systematic uncertainty.

The average B-candidate multiplicity of events that contain at least one candidate is approximately 1.02; events with three or more candidates are very rare. In events with more than one candidate, we retain the candidate with the minimum χ^2 value calculated from the measured and known values of $m\left(K_S^0 h^+ h^-\right)$ and m_{bc} as well as the respective experimental resolutions; studies using simulated samples of signal decays show that this criterion selects the correctly reconstructed candidate approximately 65% of the time for all the decay modes. The selection efficiencies are summarised in table 1. The $B^+ \to D\left(K_S^0 \pi^+ \pi^-\right) h^+$ selection efficiency is marginally improved at Belle II compared to Belle, whereas there is a significant improvement in the $B^+ \to D\left(K_S^0 K^+ K^-\right) h^+$ selection efficiency. This increase is due to the $\mathcal{R}_{K/\pi} > 0.2$ requirement on the D-decay products being more efficient when applied to Belle II data compared to Belle data.

6 $x_{\pm}^{DK}$ and $y_{\pm}^{DK}$ determination from $B^+ \to Dh^+$ decays

We perform a simultaneous analysis of $B^+ \to DK^+$ and $B^+ \to D\pi^+$ decays. The $B^+ \to DK^+$ sample provides almost all of the sensitivity to CP violation, whereas $B^+ \to D\pi^+$ is primarily used to constrain the F_i fractions. Furthermore, the $B^+ \to D\pi^+$ background in the $B^+ \to DK^+$ sample due to K-π misidentification can be directly determined from the simultaneous analysis of these two decay channels. The whole $B^+ \to Dh^+$ sample is divided into pion- and kaon-enhanced categories by applying the requirements $\mathcal{R}_{K/\pi} < 0.6$ and $\mathcal{R}_{K/\pi} > 0.6$ to the h^+, respectively.

The signal extraction involves a two-dimensional fit of the ΔE and C' distributions. The latter variable is related to C, the output of the FastBDT, which is difficult to model analytically. We transform C to C' using an ordered list of C values from the signal simulation sample such that C' is the fraction of signal events present below a given value of C in the list [51]. Therefore, the signal distribution of C' is uniform between zero and one. In practice, due to small differences in the FastBDT-input-variable distributions between data and simulation, the signal is described by a straight line in data. The background C' distribution peaks at zero and is modelled by an exponential.

Along with the signal component, we have the following three background components in our fit:

- $q\bar{q}$ background events;

- $B\bar{B}$ background events, coming from misreconstructed candidates from $e^+e^- \to \Upsilon(4S) \to B\bar{B}$ decays; and

- peaking background from $B^+ \to Dh^+$, $(h = \pi \text{ or } K)$ decays due to K-π misidentification.

The two-dimensional probability density function (PDF) for each component is the product of the one-dimensional PDFs for ΔE and C'. Negligible correlations between ΔE and C' in simulation samples support the validity of this assumption. To test whether there is any non-linear correlation, the fits are performed on simulated samples and no significant bias between the measured and generated parameters is observed, which also indicates there is negligible correlation.

The $B^+ \to D\left(K_S^0 \pi^+ \pi^-\right) h^+$ signal components are modelled with a sum of two Gaussian functions and an asymmetric Gaussian function for ΔE, and a straight line for C'. These PDFs are common to both kaon- and pion-enhanced samples. The common mean of the ΔE functions and the slope of the straight line are extracted directly from the data, along with a scaling factor to the narrowest signal Gaussian to account for any difference in ΔE resolution between simulated and data samples; other parameters are fixed to those obtained from a fit to a large simulated sample of signal events.

The $q\bar{q}$ background is modelled with a straight line for ΔE and a sum of two exponentials for C'. The slope of the straight line and the steeper exponential function's exponent are determined from the fit to data; other parameters are fixed to those obtained from a

fit to the corresponding simulated sample. These PDFs are common to both pion- and kaon-enhanced samples.

The misreconstructed $B\bar{B}$ background distribution is slightly different for pion- and kaon-enhanced samples so they are modelled separately. The ΔE (C') PDFs are an exponential (straight line) and a sum of an exponential and straight line (second-order polynomial), for the pion- and kaon-enhanced samples, respectively. Only the slope of the kaon-enhanced ΔE PDF is determined from the fit. The PDF descriptions of the peaking backgrounds are the same as those of the signal components but with independent parameters.

For the $B^+ \to D\left(K_S^0 K^+ K^-\right)h^+$ final state, some component PDFs are modified. The $B\bar{B}$ background PDFs that describes ΔE and C' for the kaon-enhanced sample are an exponential and a straight line, respectively; the slope of the exponential is a free parameter. The $q\bar{q}$ background of both samples is modelled with just a single exponential function. All other component PDFs are the same as those for the $B^+ \to D\left(K_S^0 \pi^+ \pi^-\right)h^+$ final state.

The PDF parameterisation is identical for the fits to the Belle and Belle II data samples; only the fixed parameter values are estimated separately from the simulation samples corresponding to the respective experiments. First, we perform separate fits to the Belle and Belle II data samples, which are subdivided based on the reconstructed D-decay final state. These fits are to data integrated over the D-decay Dalitz plot. We refer to this fit as the "combined fit". The signal and peaking background yields $N_{h'}^{Dh}$, where $h' = \pi$ or K represents the respective enhancement of the sample, are parameterised in terms of kaon-identification efficiency (ϵ) and K-π misidentification rate (κ) using the relations

$$N_\pi^{D\pi} = (1 - \kappa)N_{\text{tot}}^{D\pi},$$
$$N_\pi^{DK} = (1 - \epsilon)N_{\text{tot}}^{DK},$$
$$N_K^{DK} = \epsilon N_{\text{tot}}^{DK}, \text{ and}$$
$$N_K^{D\pi} = \kappa N_{\text{tot}}^{D\pi},$$

where $N_{\text{tot}}^{D\pi}$ and N_{tot}^{DK} represent the total $D\pi$ and DK yields without any PID selection, respectively. In this way, κ is directly extracted from data. The value of ϵ is fixed to the value determined from data control samples of $D^{*+} \to D^0\left(K^-\pi^+\right)\pi^+$ decays. The total signal and background yields obtained from the combined fit are summarised in table 2. Distributions restricted to candidates with $|\Delta E| < 0.05\,\text{GeV}$ and $0.65 < C' < 1$ (signal-enhanced) are shown in figures 2–5 with fit projections overlaid.

To determine the CP-violating observables, we further divide the fit categories according to the charge of B candidates and the D-decay Dalitz bins described in section 2. This fit is performed simultaneously for the Belle and Belle II data and is referred to as the "binned fit". The component PDFs for the individual bins are the same as in the fits to the unbinned data, along with the same sets of free and fixed parameters. The value of κ is fixed in the binned fit to that obtained from the combined fit. The signal yield in each bin is parameterised according to the expressions in eq. (2.3), which depend on common $x_\pm^{DK}, y_\pm^{DK}, x_\xi^{D\pi}$ and $y_\xi^{D\pi}$ parameters, as well as the external input values of c_i and s_i [16, 17]. The background yields are fit independently in each bin for both B^+ and B^- samples, which

	Sample	Pion-enhanced		Kaon-enhanced	
D decay	Component	Belle	Belle II	Belle	Belle II
$D \to K_S^0 \pi^+ \pi^-$	$B^+ \to D\pi^+$	21325 ± 162	4193 ± 70	1764 ± 64	308 ± 23
	$B^+ \to DK^+$	140 ± 29	62 ± 11	1467 ± 53	280 ± 21
	$B\bar{B}$ background	5040 ± 155	1223 ± 68	1309 ± 85	387 ± 42
	$q\bar{q}$ background	9022 ± 172	1657 ± 69	6295 ± 122	1021 ± 47
$D \to K_S^0 K^+ K^-$	$B^+ \to D\pi^+$	2740 ± 56	519 ± 21	211 ± 18	50 ± 10
	$B^+ \to DK^+$	17 ± 4	2.1 ± 0.2	194 ± 17	34 ± 7
	$B\bar{B}$ background	333 ± 31	77 ± 12	110 ± 18	22 ± 7
	$q\bar{q}$ background	409 ± 37	124 ± 14	309 ± 28	92 ± 11

Table 2. Signal and background yields obtained from the two-dimensional combined fit.
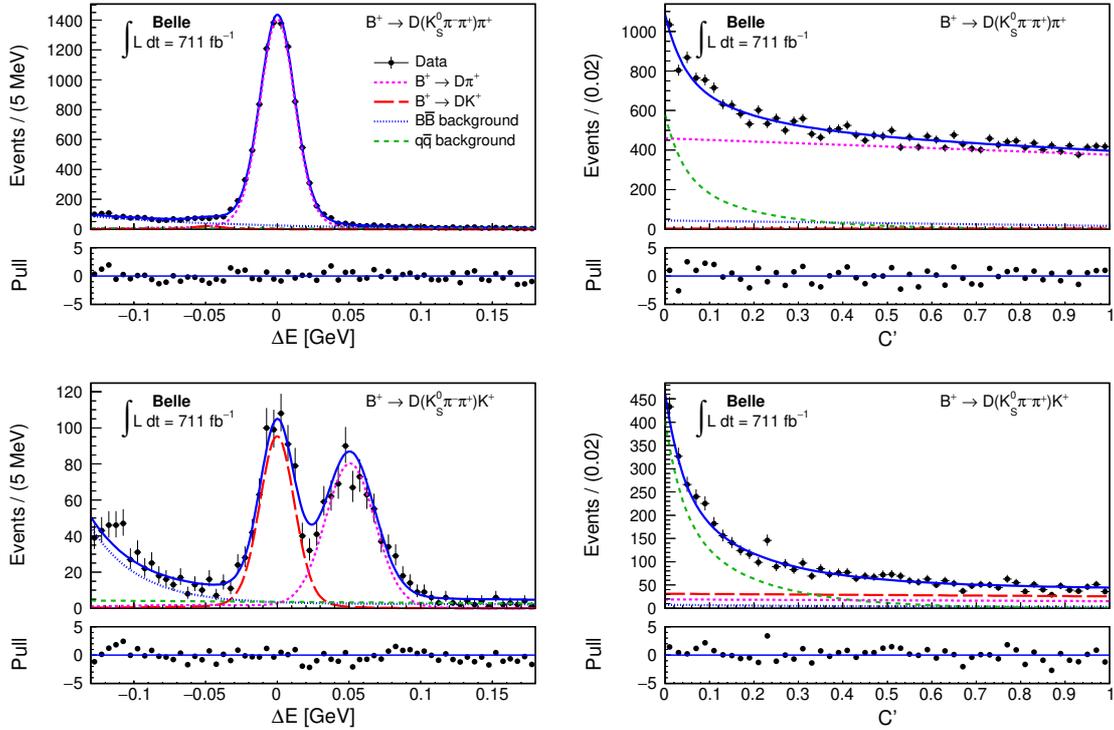
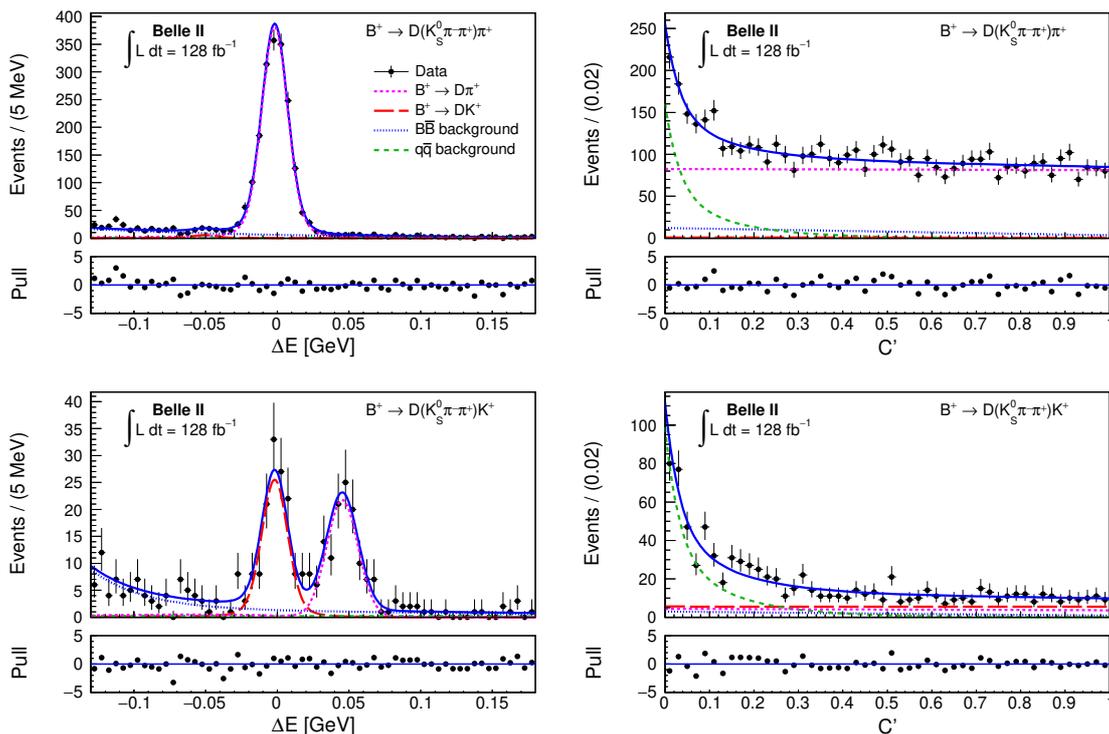**Figure 2**. Distributions of (left) ΔE and (right) C' for (top) $B^+ \to D(K_S^0 \pi^- \pi^+)\pi^+$ and (bottom) $B^+ \to D(K_S^0 \pi^- \pi^+)K^+$ candidates restricted to the signal-enhanced region in the Belle data set with fit projections overlaid. The black points with error bars represent data and the solid blue curve is the total fit. The large-dotted magenta, long-dashed red, small-dotted blue and short-dashed green curves represent $B^+ \to D\pi^+$, $B^+ \to DK^+$, $q\bar{q}$ and combinatorial $B\bar{B}$ background components, respectively. Differences between the fit function and data normalised by the uncertainty in data (pull) are shown under each panel.
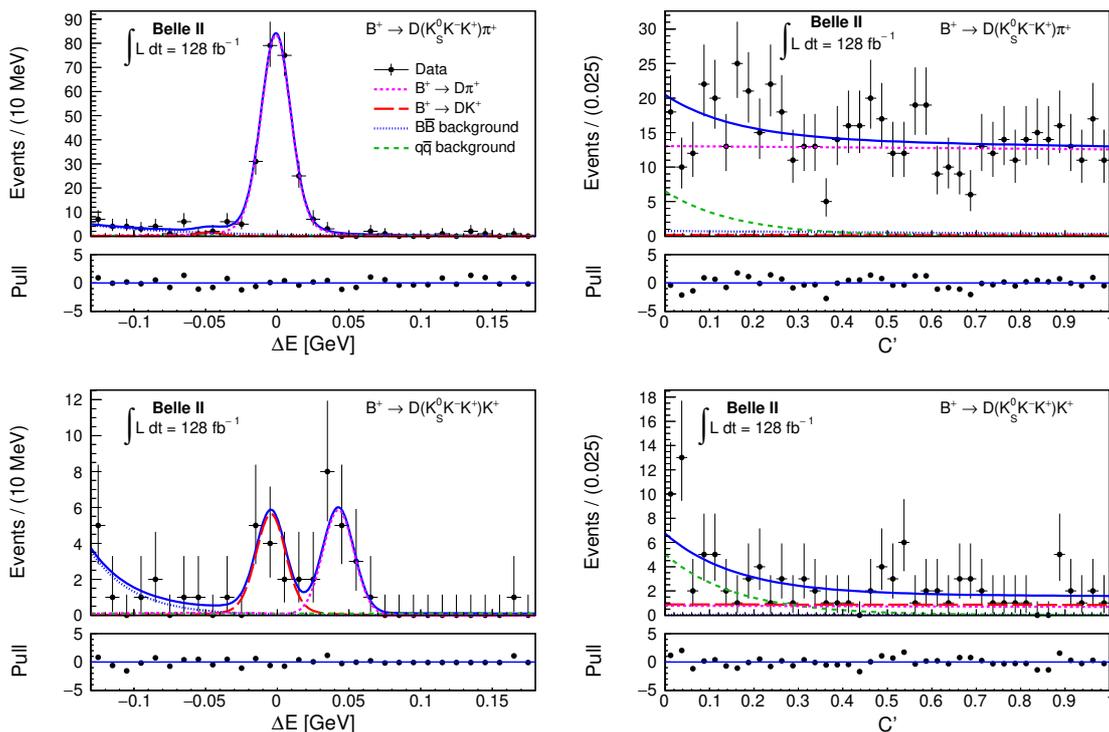
Figure 3. Distributions of (left) ΔE and (right) C' for (top) $B^+ \to D(K_S^0 K^- K^+)\pi^+$ and (bottom) $B^+ \to D(K_S^0 K^- K^+)K^+$ candidates restricted to the signal-enhanced region in the Belle data set with fit projections overlaid. The black points with error bars represent data and the solid blue curve is the total fit. The large-dotted magenta, long-dashed red, small-dotted blue and short-dashed green curves represent $B^+ \to D\pi^+$, $B^+ \to DK^+$, $q\bar{q}$ and combinatorial $B\bar{B}$ background components, respectively. Differences between the fit function and data normalised by the uncertainty in data (pull) are shown under each panel.

accounts for any CP-violation in the background. The F_i and F_{-i} fractions are extracted directly from the fit. As these fractions must satisfy $\sum F_i = 1, F_i \in [0, 1]$, a fit instability can be induced due to large correlations between the F_i parameters [7]. Hence, following ref. [7], we reparameterise F_i as a series of $2\mathcal{N} - 1$ recursive fractions $\mathcal{R}_i$ that are extracted from the fit. The $\mathcal{R}_i$ fractions are defined as

$$
F_i = \begin{cases} \mathcal{R}_i & , \quad i = -\mathcal{N} \\ \mathcal{R}_i \prod_{j<i}(1 - \mathcal{R}_j) & , \quad -\mathcal{N} < i < +\mathcal{N} \\ \prod_{j<i}(1 - \mathcal{R}_j) & , \quad i = +\mathcal{N}. \end{cases} \tag{6.1}
$$

The values of $\mathcal{R}_i$ are independent for Belle and Belle II such that any difference in the acceptance profile is accounted for. The values of $\mathcal{R}_i$ are found to be compatible between Belle and Belle II. However, if common $\mathcal{R}_i$ parameters are used, there is little statistical advantage in determining the CP-violating observables and an additional systematic uncertainty would be introduced related to the assumption. Figure 6 (7) shows the measured $B^+ \to Dh^+$ yields in each bin for the Belle (Belle II) data sample.

Figure 4. Distributions of (left) ΔE and (right) C' for (top) $B^+ \to D(K_S^0\pi^-\pi^+)\pi^+$ and (bottom) $B^+ \to D(K_S^0\pi^-\pi^+)K^+$ candidates restricted to the signal-enhanced region in the Belle II data set with fit projections overlaid. The black points with error bars represent data and the solid blue curve is the total fit. The large-dotted magenta, long-dashed red, small-dotted blue and short-dashed green curves represent $B^+ \to D\pi^+$, $B^+ \to DK^+$, $q\bar{q}$ and combinatorial $B\bar{B}$ background components, respectively. Differences between the fit function and data normalised by the uncertainty in data (pull) are shown under each panel.

The fit results along with their statistical and systematic uncertainties are summarised in section 8, and the likelihood contours are shown in figure 8. The correlations between the parameters are given in appendix A. The bin-by-bin asymmetries $\left(N_{-i}^- - N_{+i}^+\right)/\left(N_{-i}^- + N_{+i}^+\right)$ in each Dalitz plot bin i are shown in figure 9. Clear evidence for CP violation is seen in the Belle kaon-enhanced sample as in the earlier Belle analysis [20]. We assess the significance of the observed CP violation by comparing the likelihood to that from a fit under the no CP-violation hypothesis of $x_+^{DK} = x_-^{DK}$ and $y_+^{DK} = y_-^{DK}$. Considering only the statistical uncertainties we find the significance is 5.8 standard deviations.

7 Systematic uncertainties

Several possible sources of systematic uncertainties are considered, which are listed in table 3. This section explains each source and the methodology adopted to compute the systematic uncertainties. The only correlated sources of systematic uncertainty between Belle and Belle II are the input c_i and s_i values, as well as the fit bias. All other systematic uncertainties are assessed independently for Belle and Belle II, and are summed in quadrature.

Figure 5. Distributions of (left) ΔE and (right) C' for (top) $B^+ \to D(K_S^0 K^- K^+)\pi^+$ and (bottom) $B^+ \to D(K_S^0 K^- K^+)K^+$ candidates restricted to the signal-enhanced region in the Belle II data set with fit projections overlaid. The black points with error bars represent data and the solid blue curve is the total fit. The large-dotted magenta, long-dashed red, small-dotted blue and short-dashed green curves represent $B^+ \to D\pi^+$, $B^+ \to DK^+$, $q\bar{q}$ and combinatorial $B\bar{B}$ background components, respectively. Differences between the fit function and data normalised by the uncertainty in data (pull) are shown under each panel.

In general, we smear the input nominal values by their uncertainties and then perform a fit to assess the associated systematic uncertainty. The smearing procedure is repeated 1000 times and the resulting width of the fit parameter distribution from this ensemble of fits is considered as the corresponding systematic uncertainty. If the input values are correlated, we use the Cholesky decomposition [52] of the covariance matrix to smear the uncertainties, which takes the correlation into account. This approach is used to compute the contributions of the external inputs c_i and s_i, and any correlated fixed parameters used to describe the PDFs. The correlations of the external inputs are taken from refs. [16, 17]. The correlations between the fixed fit parameters are taken from the results of fits to simulated samples of the signal and background components.[7] The results are listed in table 3. The corresponding uncertainties are less than 20% and 5% of the total statistical uncertainty for the external inputs and the fixed fit parameters, respectively. The systematic

---

[7]We provide the detailed output of this study as supplementary material to this paper at the publisher's website, as noted in ref. [7] this will provide sufficient information to determine the correlation between this uncertainty and the corresponding uncertainties of other ϕ_3 measurements that also rely on the same strong-phase measurements.
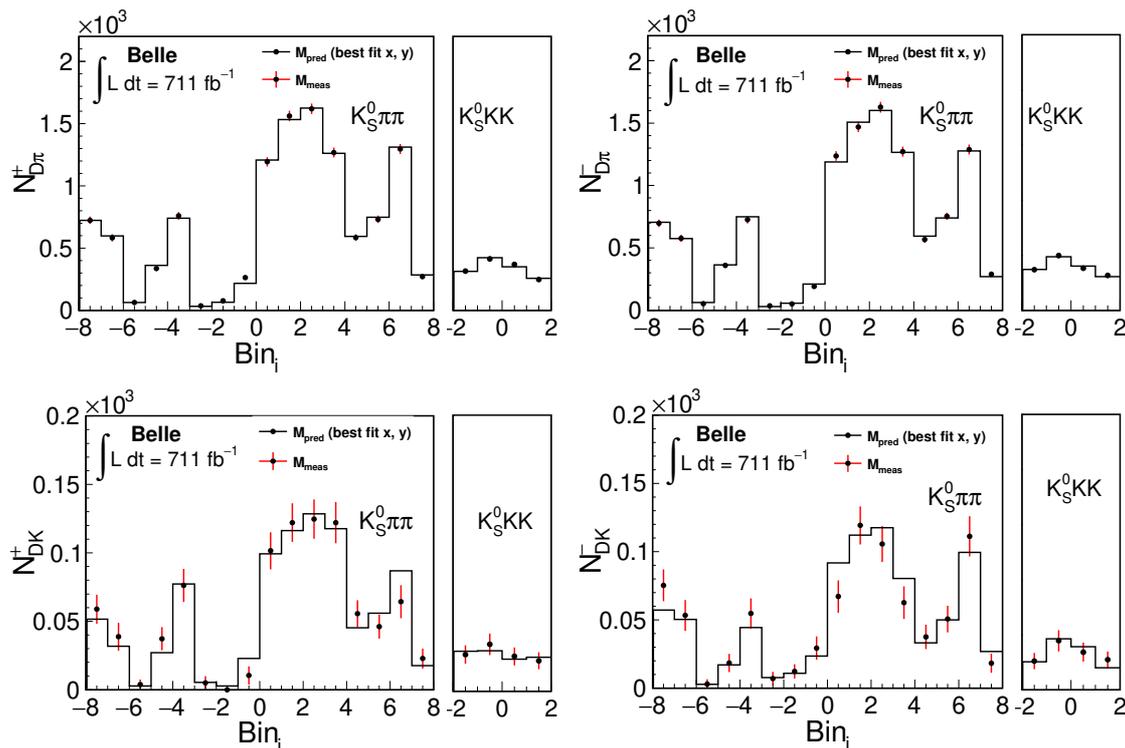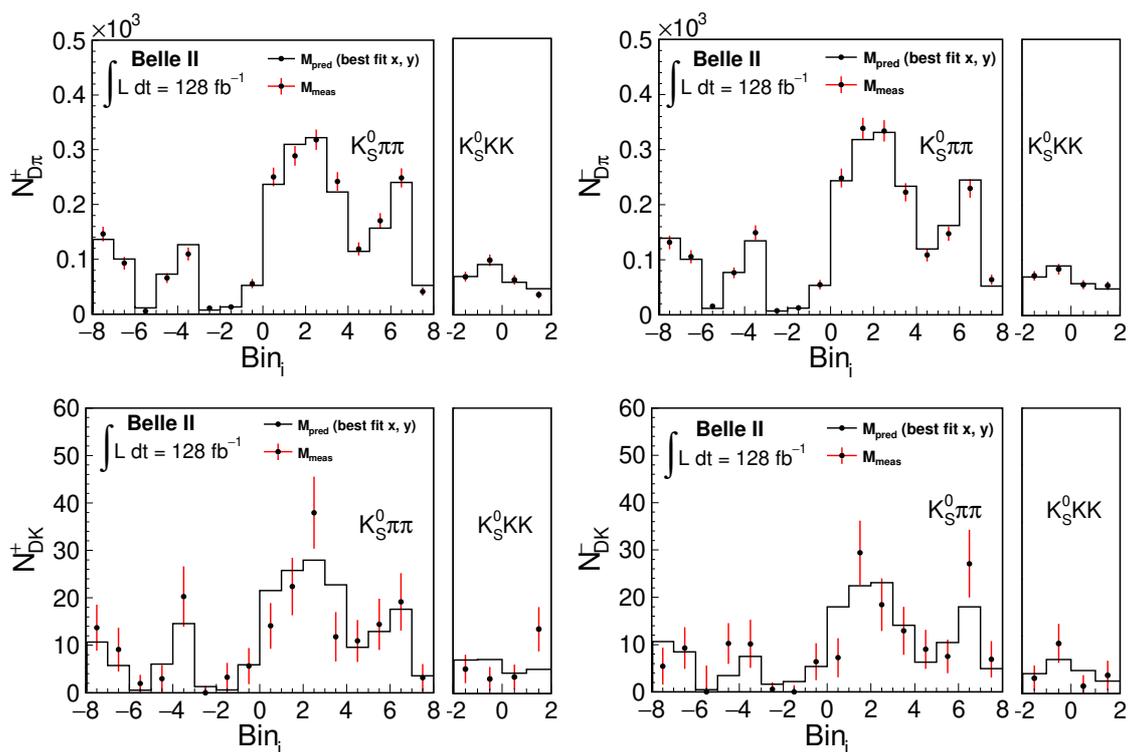
Figure 6. Yields in bins for $B^+ \to D\pi^+$ (top left), $B^- \to D\pi^-$ (top right), $B^+ \to DK^+$ (bottom left) and $B^- \to DK^-$ (bottom right) decays in the Belle data set. The data points with error bars are the measured yields with their statistical uncertainty and the histogram is the expected yield from the best fit $(x_\pm, y_\pm)$ parameter values.

uncertainties related to PID are also calculated using this same strategy, where the efficiency and misidentification rates are varied within their uncertainty, independently for Belle and Belle II. To estimate the effect of ignoring the charmless peaking background we repeat the fits include a fixed peaking background component normalised to the yields found in the studies of the $m\left(K_S^0 h^+ h^-\right)$ sideband. The background is modelled using the same PDF distributions as the signal. The resulting bias in the central values of the physics parameters, which is two orders of magnitude smaller than the statistical uncertainty, is considered as a systematic uncertainty.

Fit biases are investigated using linearity tests. Many simulated data sets of bin yields are generated for five different values of $x_\pm^{DK}$, $y_\pm^{DK}$, $x_\xi^{D\pi}$ and $y_\xi^{D\pi}$: $0, \pm 0.05$ and ± 0.1. Each sample is then fit to determine the parameters. For an unbiased sample a graph of generated versus fit values should be linear with slope one and intercept zero. No significant bias is observed. The slopes agree with unity except for $x_\xi^{D\pi}$, which differs by three standard deviations. As this is a nuisance parameter in the fit, it has no impact on the final ϕ_3 extraction. The associated systematic uncertainty is assessed using the uncertainty in the slope and the data central values.

We also check the contribution of migration between D-decay Dalitz plot bins due to the finite resolution of $m_\pm^2$. The definition of F_i includes the effect of migration if it is the same in the $B^+ \to D\pi^+$ and $B^+ \to DK^+$ samples. However, the presence of CP violation

Figure 7. Yields in bins for $B^+ \to D\pi^+$ (top left), $B^- \to D\pi^-$ (top right), $B^+ \to DK^+$ (bottom left) and $B^- \to DK^-$ (bottom right) decays in the Belle II data set. The data points with error bars are the measured yields with their statistical uncertainty and the histogram is the expected yield from the best fit $(x_\pm, y_\pm)$ parameter values.
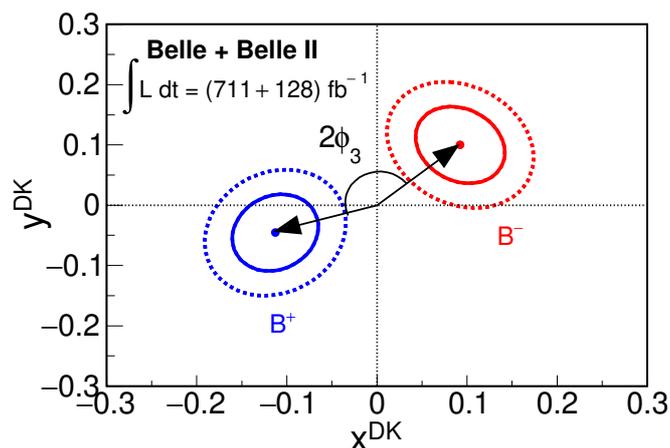
Figure 8. Two-dimensional confidence regions at (inner curve) 68.3% and (outer curve) 95.5% probability for $\left(x_+^{DK}, y_+^{DK}\right)$ (blue) and $\left(x_-^{DK}, y_-^{DK}\right)$ (red) as measured in $B^+ \to DK^+$ decays from a profile likelihood scan. The dots represent central values.
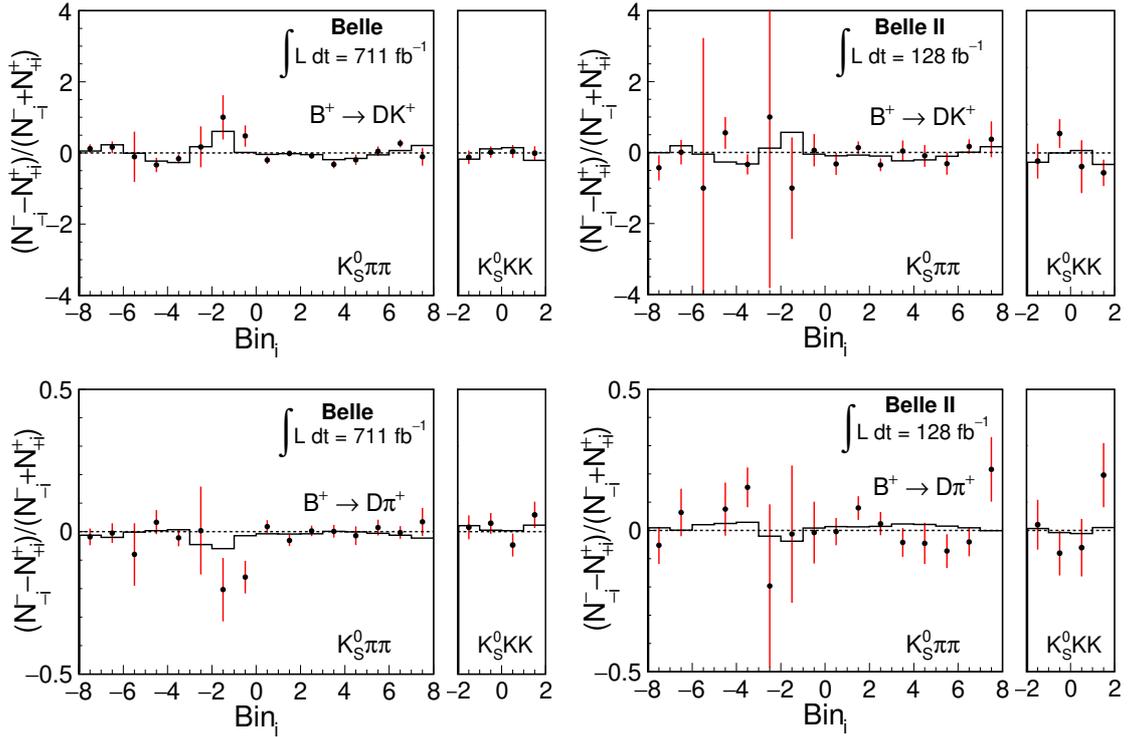
Figure 9. Per-bin yield asymmetries $\left(N_{-i}^{-} - N_{+i}^{+}\right) / \left(N_{-i}^{-} + N_{+i}^{+}\right)$ in each Dalitz plot bin i for $B^{+} \to DK^{+}$ (top) and $B^{+} \to D\pi^{+}$ (bottom) for the Belle (left) and Belle II (right) data sets. The asymmetries produced in fits with independent bin yields are given with statistical error bars, and the prediction from the best-combined-fit values of the (x, y) parameters is displayed with a solid line. The dotted line is the expectation without CP violation.

Source	$\sigma_{x_+^{DK}}$	$\sigma_{y_+^{DK}}$	$\sigma_{x_-^{DK}}$	$\sigma_{y_-^{DK}}$	$\sigma_{x_\xi^{D\pi}}$	$\sigma_{y_\xi^{D\pi}}$
Input c_i, s_i	0.22	0.55	0.23	0.67	0.73	0.82
PDF parametrisation	0.07	0.08	0.12	0.16	0.12	0.12
PID	< 0.01	< 0.01	< 0.01	0.01	< 0.01	< 0.01
Peaking background	0.03	0.05	0.03	0.04	0.02	0.10
Fit bias	0.16	0.06	0.12	0.16	0.49	0.10
Bin migration	< 0.01	< 0.01	< 0.01	< 0.01	< 0.01	0.03
Total	0.18	0.11	0.17	0.23	0.51	0.19
Statistical	3.15	4.20	3.27	4.20	4.75	5.44

Table 3. Systematic uncertainty summary. All values are quoted in units of 10^{-2}.

means the Dalitz plot densities of the two samples are different, which can lead to differing levels of migration. Therefore, we generate samples of events including CP violation and fit them with and without the effect of $m_{\pm}^{2}$ resolution included. The parameter values shift less than 10^{-4} except for $y_{\xi}^{D\pi}$; the full bias is treated as a systematic uncertainty on $y_{\xi}^{D\pi}$.

We assume that the values of F_i are the same for $B^{+} \to D\left(K_{S}^{0}h^{+}h^{-}\right)K^{+}$ and $B^{-} \to \left(K_{S}^{0}h^{+}h^{-}\right)\pi^{+}$ decays. In principle a small difference exists due to the altered

kinematics induced by the differing pion and kaon masses. We investigated the validity of our assumption in large simulated samples. No significant difference is observed in the values of F_i so no related systematic uncertainty is assigned. We also consider how the Belle and Belle II Dalitz plot acceptance might distort the effective values of c_i and s_i, which are measured assuming a uniform acceptance. The values are calculated with and without the Belle (Belle II) acceptance included. The deviations in the values of c_i and s_i are at most an order of magnitude smaller than the reported uncertainties [16, 17], which are already considered in our measurement. Therefore, this potential source of systematic uncertainty is ignored.

As a further check of the fit performance, we generate 1000 simplified-simulated experiments with mean signal yields that correspond to our measured values of CP-violating parameters. These samples are then fit in an identical manner to the data. The results verify that the fit is stable and unbiased with the current sample size, as well as providing the appropriate statistical coverage. We also find that the uncertainties on measured CP-violating parameters in data lie within the distribution of uncertainties generated by the simplified-simulated experiments.

8   Determination of ϕ_3, r_B^{DK} and δ_B^{DK}

The parameters obtained from the fit are

$$
\begin{aligned}
x_-^{DK} &= (\quad 9.24 \pm 3.27 \pm 0.17 \pm 0.23) \times 10^{-2}, \\
y_-^{DK} &= (\quad 10.00 \pm 4.20 \pm 0.23 \pm 0.67) \times 10^{-2}, \\
x_+^{DK} &= (-11.28 \pm 3.15 \pm 0.18 \pm 0.22) \times 10^{-2}, \\
y_+^{DK} &= (\quad -4.55 \pm 4.20 \pm 0.11 \pm 0.55) \times 10^{-2}, \\
x_\xi^{D\pi} &= (-11.09 \pm 4.75 \pm 0.51 \pm 0.73) \times 10^{-2}, \\
y_\xi^{D\pi} &= (\quad -7.90 \pm 5.44 \pm 0.19 \pm 0.82) \times 10^{-2},
\end{aligned}
\tag{8.1}
$$

where the first uncertainty is statistical, the second is the total experimental systematic uncertainty, and the third is the systematic uncertainty due to the external strong-phase difference inputs [16, 17].

The parameters $\phi_3, r_B^{DK}, \delta_B^{DK}, r_B^{D\pi}$ and $\delta_B^{D\pi}$ are determined from $x_\pm^{DK}, y_\pm^{DK}, x_\xi^{D\pi}$ and $y_\xi^{D\pi}$ using a frequentist approach implemented in the GAMMACOMBO package [53].[8] Generally, there is a two-fold ambiguity in the results of these physics parameters as eqs. (2.3) are invariant under the simultaneous substitutions of $\phi_3 = \phi_3 + 180°$ and $\delta_B^{Dh} = \delta_B^{Dh} + 180°$. We choose the solution in the range $0° < \phi_3 < 180°$, which is favoured by other measurements [5].[2] The results are

$$
\begin{aligned}
\phi_3 &= (78.4 \pm 11.4 \pm 0.5 \pm 1.0)°, \\
r_B^{DK} &= 0.129 \pm 0.024 \pm 0.001 \pm 0.002, \\
\delta_B^{DK} &= (124.8 \pm 12.9 \pm 0.5 \pm 1.7)°, \\
r_B^{D\pi} &= 0.017 \pm 0.006 \pm 0.001 \pm 0.001, \\
\delta_B^{D\pi} &= (341.0 \pm 17.0 \pm 1.2 \pm 2.6)°.
\end{aligned}
\tag{8.2}
$$

---

[8]Of the methods available in GAMMACOMBO, we adopt the so-called plug-in method, which uses simulated samples and assumes the nuisance parameter values observed in data.
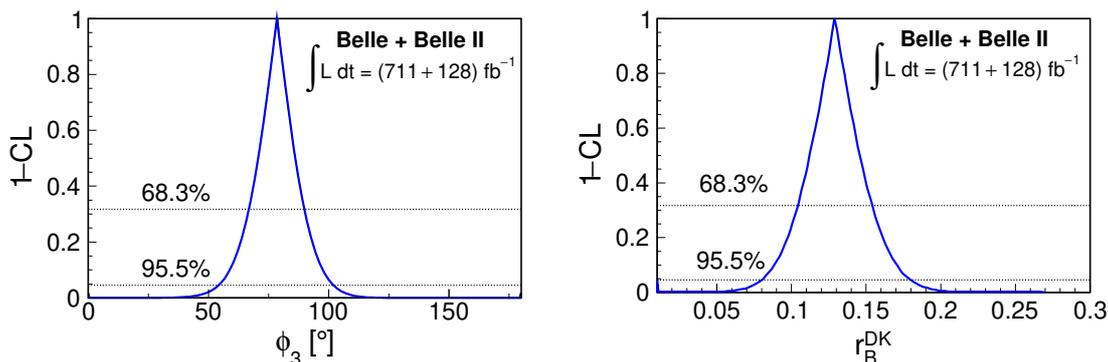
Figure 10. *p*-value as a function of (left) ϕ_3 and (right) r_B^{DK} calculated using the methods described in ref. [53].
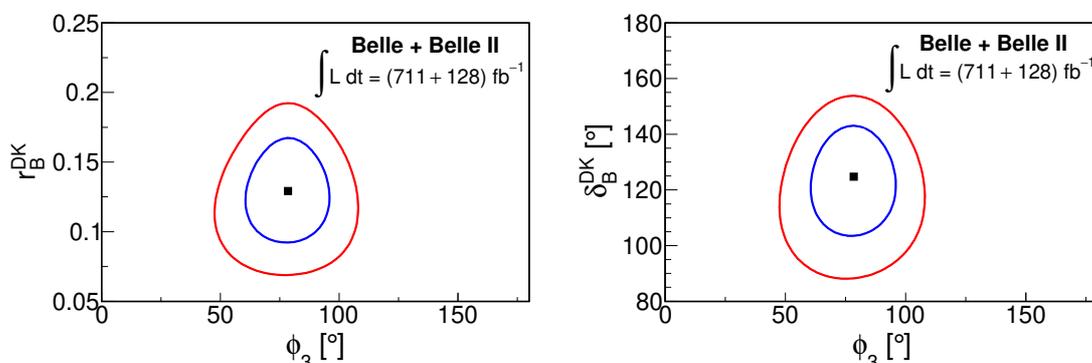

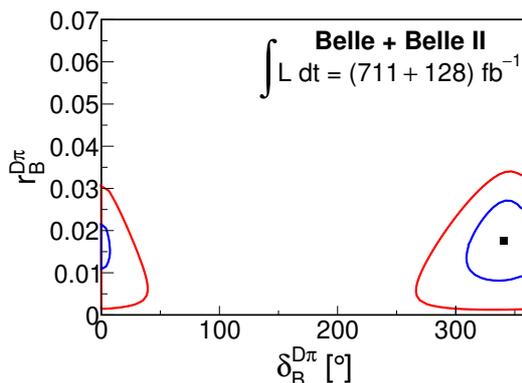**Figure 11**. Two-dimensional confidence regions at the (inner curve) 68% and (outer curve) 95%, obtained for (left) $\phi_3 - r_B^{DK}$ and (right) $\phi_3 - \delta_B^{DK}$ using the methods described in ref. [53]. Note the suppressed zeroes on the vertical scales.

The statistical confidence intervals for ϕ_3 and r_B^{DK} are illustrated in figure 10, while figure 11 shows the two-dimensional statistical confidence regions obtained for the (ϕ_3, r_B^{DK}) and (ϕ_3, δ_B) parameter combinations. Figure 12 shows the two-dimensional statistical confidence region obtained for the $(\delta_B^{D\pi}, r_B^{D\pi})$ parameter combination; the 95% confidence region is compatible with the most precise values of these parameters reported [54]. The ϕ_3 result is consistent with the previous Belle analysis [20] but the statistical precision on ϕ_3 is improved from 15° due to improved K_S^0 selection and background suppression. The uncertainty related to strong-phase inputs has also decreased from 4° because of the new measurements reported by the BESIII collaboration [16, 17]. Furthermore, the experimental systematic uncertainty is decreased from 4° primarily from the improved background suppression and the use of the $B^+ \to D\pi^+$ sample to determine the acceptance.

Figure 12. Two-dimensional confidence regions at the (inner curve) 68% and (outer curve) 95%, obtained for $\delta_B^{D\pi} - r_B^{D\pi}$ ref. [53].

9 Conclusion

The results of the first Belle and Belle II combined model-independent measurement of the CKM unitarity triangle angle ϕ_3 are presented. The analysis uses $B^+ \to D(K_S^0 h^- h^+)h^+$ decays reconstructed from a combined sample of $711\,\mathrm{fb}^{-1}$ of Belle data and $128\,\mathrm{fb}^{-1}$ of Belle II data. Independently measured strong-phase difference parameters c_i and s_i are used, which come from a combination of results reported by the CLEO and BESIII collaborations [16, 17]. We measure $\phi_3 = (78.4 \pm 11.4 \pm 0.5 \pm 1.0)^\circ$, where the first uncertainty is statistical, the second is the total experimental systematic uncertainty and the third is the systematic uncertainty due to the external c_i and s_i measurements.

The measurement is also performed on the Belle data sample alone and the results are reported in appendix B. The statistical uncertainty in ϕ_3 is 11°, which is significantly improved from the 15° reported in the previous Belle analysis with the same data set [20]. The improvements are primarily due to the improved background rejection and K_S^0 selection, as well as the addition of $B^+ \to D(K_S^0 K^+ K^-)h^+$ decays. The inclusion of Belle II data improves the precision of $x_\pm^{DK}$ and $y_\pm^{DK}$ parameters. However, the ϕ_3 statistical uncertainty does not improve despite adding 17% more data. Belle II data favours a much smaller value of r_B^{DK}, which results in a central value of 0.129 for the combined fit compared to 0.144 for the Belle data alone. The uncertainty in ϕ_3 is inversely proportional to r_B, which explains the lack of improvement in ϕ_3 sensitivity when including the Belle II data. The world average value of r_B is 0.0996 ± 0.0026 [5][2] so it is possible that the value of r_B will decrease and approach this value as additional data is included.

The statistical precision on ϕ_3 is worse than the current world-average value [5].[2] However, the precision is limited by the size of the data sample, so a future analysis with a Belle II data set corresponding to $10\,\mathrm{ab}^{-1}$ will provide measurements with a precision of approximately 4° from the $B^+ \to D\left(K_S^0 \pi^+ \pi^-\right) h^+$ mode alone.[9] The use of other modes will give additional sensitivity to ϕ_3 [55].

---

[9]The world-average value of r_B^{DK} is assumed in these extrapolations.

A   Correlation matrices

Tables 4–6 represent the statistical, external strong phase input systematics and total experimental systematics correlation matrices for the combined data set of Belle and Belle II.

	x_-^{DK}	y_-^{DK}	x_+^{DK}	y_+^{DK}	$x_\xi^{D\pi}$	$y_\xi^{D\pi}$
x_-^{DK}	1	-0.204	-0.051	0.063	0.365	-0.151
y_-^{DK}		1	0.014	-0.051	-0.090	0.404
x_+^{DK}			1	0.152	-0.330	-0.057
y_+^{DK}				1	0.026	-0.391
$x_\xi^{D\pi}$					1	0.080
$y_\xi^{D\pi}$						1

Table 4. Statistical correlation matrix obtained for the combined Belle and Belle II data set.

	x_-^{DK}	y_-^{DK}	x_+^{DK}	y_+^{DK}	$x_\xi^{D\pi}$	$y_\xi^{D\pi}$
x_-^{DK}	1	-0.113	0.069	0.406	-0.016	0.114
y_-^{DK}		1	0.038	-0.196	-0.692	-0.106
x_+^{DK}			1	0.412	-0.226	-0.469
y_+^{DK}				1	0.180	-0.069
$x_\xi^{D\pi}$					1	0.622
$y_\xi^{D\pi}$						1

Table 5. External inputs c_i, s_i systematics correlation matrix obtained for the combined Belle and Belle II data set.

	x_-^{DK}	y_-^{DK}	x_+^{DK}	y_+^{DK}	$x_\xi^{D\pi}$	$y_\xi^{D\pi}$
x_-^{DK}	1	0.777	0.483	0.268	0.839	0.698
y_-^{DK}		1	0.411	0.504	0.802	0.797
x_+^{DK}			1	0.680	0.766	0.377
y_+^{DK}				1	0.480	0.303
$x_\xi^{D\pi}$					1	0.638
$y_\xi^{D\pi}$						1

Table 6. Experimental systematics correlation matrix obtained for the combined Belle and Belle II data set.

B   Belle data results

The results obtained using only Belle data set are summarised in this section. The obtained values of the *CP* violating parameters are

$$
\begin{aligned}
x_-^{DK} &= (\quad 9.45 \pm 3.58 \pm 0.22 \pm 0.36) \times 10^{-2}, \\
y_-^{DK} &= (\ 12.04 \pm 4.66 \pm 0.30 \pm 0.90) \times 10^{-2}, \\
x_+^{DK} &= (-11.94 \pm 3.46 \pm 0.23 \pm 0.37) \times 10^{-2}, \\
y_+^{DK} &= (\ -6.34 \pm 4.75 \pm 0.17 \pm 0.93) \times 10^{-2}, \\
x_\xi^{D\pi} &= (\ -8.76 \pm 4.50 \pm 0.50 \pm 0.69) \times 10^{-2}, \\
y_\xi^{D\pi} &= (\ -4.56 \pm 4.90 \pm 0.17 \pm 0.63) \times 10^{-2}.
\end{aligned}
\tag{B.1}
$$

The obtained physics parameters values are

$$
\begin{aligned}
\phi_3 &= (79.3 \pm 11.0 \pm 0.6 \pm 1.4)^\circ. \\
r_B^{DK} &= 0.144 \pm 0.028 \pm 0.002 \pm 0.004, \\
\delta_B^{DK} &= (130.1 \pm 12.4 \pm 0.6 \pm 2.2)^\circ. \\
r_B^{D\pi} &= 0.014 \pm 0.007 \pm 0.001 \pm 0.001, \\
\delta_B^{D\pi} &= (337.5 \pm 22.0 \pm 1.3 \pm 2.9)^\circ.
\end{aligned}
\tag{B.2}
$$

The correlation matrices related to statistical, external strong phase input systematics, and total experimental systematics are given in tables 7–9.

	x_-^{DK}	y_-^{DK}	x_+^{DK}	y_+^{DK}	$x_\xi^{D\pi}$	$y_\xi^{D\pi}$
x_-^{DK}	1	−0.205	−0.054	0.031	0.245	−0.167
y_-^{DK}		1	0.000	−0.045	0.033	0.315
x_+^{DK}			1	0.167	−0.298	−0.017
y_+^{DK}				1	0.103	−0.323
$x_\xi^{D\pi}$					1	0.184
$y_\xi^{D\pi}$						1

Table 7. Statistical correlation matrix obtained for the Belle standalone data set.

	x_-^{DK}	y_-^{DK}	x_+^{DK}	y_+^{DK}	$x_\xi^{D\pi}$	$y_\xi^{D\pi}$
x_-^{DK}	1	0.095	0.333	0.575	0.383	0.396
y_-^{DK}		1	0.279	−0.054	−0.538	−0.328
x_+^{DK}			1	0.475	0.048	−0.222
y_+^{DK}				1	0.420	0.295
$x_\xi^{D\pi}$					1	0.862
$y_\xi^{D\pi}$						1

Table 8. External inputs c_i, s_i systematics correlation matrix obtained for the Belle standalone data set.

	x_-^{DK}	y_-^{DK}	x_+^{DK}	y_+^{DK}	$x_\xi^{D\pi}$	$y_\xi^{D\pi}$
x_-^{DK}	1	0.508	0.251	0.074	0.674	0.573
y_-^{DK}		1	0.109	0.071	0.661	0.683
x_+^{DK}			1	0.467	0.589	0.324
y_+^{DK}				1	0.254	0.125
$x_\xi^{D\pi}$					1	0.724
$y_\xi^{D\pi}$						1

Table 9. Experimental systematics correlation matrix obtained for the Belle standalone data set.

Acknowledgments

References

[1] N. Cabibbo, *Unitary Symmetry and Leptonic Decays*, *Phys. Rev. Lett.* **10** (1963) 531 [INSPIRE].

[2] M. Kobayashi and T. Maskawa, *CP violation in the renormalizable theory of weak interaction*, *PTEP* **49** (1973) 652 [INSPIRE].

[3] J. Brod and J. Zupan, *The ultimate theoretical error on γ from $B \to DK$ decays*, *JHEP* **01** (2014) 051 [arXiv:1308.5663] [INSPIRE].

[4] M. Blanke and A.J. Buras, *Emerging ΔM_d-anomaly from tree-level determinations of $|V_{cb}|$ and the angle γ*, *Eur. Phys. J. C* **79** (2019) 159 [arXiv:1812.06963] [InSPIRE].

[5] HFLAV collaboration, *Averages of b-hadron, c-hadron, and τ-lepton properties as of 2018*, *Eur. Phys. J. C* **81** (2021) 226 [arXiv:1909.12524] [InSPIRE].

[6] D. King, M. Kirk, A. Lenz and T. Rauh, *$|V_{cb}|$ and γ from B-mixing — Addendum to "B_s mixing observables and $|V_{td}/V_{ts}|$ from sum rules"*, *JHEP* **03** (2020) 112 [arXiv:1911.07856] [InSPIRE].

[7] LHCb collaboration, *Measurement of the CKM angle γ in $B^{\pm} \to DK^{\pm}$ and $B^{\pm} \to D\pi^{\pm}$ decays with $D \to K_S^0 h^+ h^-$*, *JHEP* **02** (2021) 169 [arXiv:2010.08483] [InSPIRE].

[8] A. Giri, Y. Grossman, A. Soffer and J. Zupan, *Determining γ using $B^- \to DK^-$ with multibody D decays*, *Phys. Rev. D* **68** (2003) 054018 [hep-ph/0303187] [InSPIRE].

[9] A. Bondar, *Proceedings of BINP special analysis meeting on Dalitz analysis*, unpublished, 24–26 September 2002.

[10] BELLE collaboration, *Measurement of ϕ_3 with Dalitz plot analysis of $B^{\pm} \to D^{(*)}K^{\pm}$ decay*, *Phys. Rev. D* **70** (2004) 072003 [hep-ex/0406067] [InSPIRE].

[11] M. Gronau and D. Wyler, *On determining a weak phase from CP asymmetries in charged B decays*, *Phys. Lett. B* **265** (1991) 172 [InSPIRE].

[12] M. Gronau and D. London, *How to determine all the angles of the unitarity triangle from $B_d^0 \to DK_S$ and $B_S^0 \to D\phi$*, *Phys. Lett. B* **253** (1991) 483 [InSPIRE].

[13] D. Atwood, I. Dunietz and A. Soni, *Enhanced CP violation with $B \to KD^0(\bar{D}^0)$ modes and extraction of the CKM angle γ*, *Phys. Rev. Lett.* **78** (1997) 3257 [hep-ph/9612433] [InSPIRE].

[14] D. Atwood, I. Dunietz and A. Soni, *Improved methods for observing CP violation in $B^{\pm} \to K^{\pm}D$ and measuring the CKM phase gamma*, *Phys. Rev. D* **63** (2001) 036005 [hep-ph/0008090] [InSPIRE].

[15] CLEO collaboration, *Model-independent determination of the strong-phase difference between D^0 and $\bar{D}^0 \to K_{S,L}^0 h^+ h^-$ $(h = \pi, K)$ and its impact on the measurement of the CKM angle γ/ϕ_3*, *Phys. Rev. D* **82** (2010) 112006 [arXiv:1010.2817] [InSPIRE].

[16] BESIII collaboration, *Model-independent determination of the relative strong-phase difference between D^0 and $\bar{D}^0 \to K_{S,L}^0 \pi^+ \pi^-$ and its impact on the measurement of the CKM angle γ/ϕ_3*, *Phys. Rev. D* **101** (2020) 112002 [arXiv:2003.00091] [InSPIRE].

[17] BESIII collaboration, *Improved model-independent determination of the strong-phase difference between D^0 and $\bar{D}^0 \to K_{S,L}^0 K^+ K^-$ decays*, *Phys. Rev. D* **102** (2020) 052008 [arXiv:2007.07959] [InSPIRE].

[18] BaBar collaboration, *Evidence for direct CP violation in the measurement of the Cabibbo-Kobayashi-Maskawa angle gamma with $B^{\pm} \to D^{(*)}K^{(*)\pm}$ decays*, *Phys. Rev. Lett.* **105** (2010) 121801 [arXiv:1005.1096] [InSPIRE].

[19] BELLE collaboration, *Evidence for direct CP violation in the decay $B \to D^{(*)}K, D \to K_S^0 \pi^+ \pi^-$ and measurement of the CKM phase ϕ_3*, *Phys. Rev. D* **81** (2010) 112002 [arXiv:1003.3360] [InSPIRE].

[20] BELLE collaboration, *First Measurement of ϕ_3 with a Model-independent Dalitz Plot Analysis of $B^{\pm} \to DK^{\pm}, D \to K_S^0 \pi\pi$ Decay*, *Phys. Rev. D* **85** (2012) 112014 [arXiv:1204.6561] [InSPIRE].

[21] A. Di Canto et al., *Novel method for measuring charm-mixing parameters using multibody decays*, *Phys. Rev. D* **99** (2019) 012007 [arXiv:1811.01032] [INSPIRE].

[22] PARTICLE DATA GROUP collaboration, *Review of Particle Physics*, *PTEP* **2020** (2020) 083C01 [INSPIRE].

[23] J. Garra Ticó, *A strategy for a simultaneous measurement of CP violation parameters related to the CKM angle γ in multiple B meson decay channels*, arXiv:1804.05597 [INSPIRE].

[24] J. Garra Ticó, V. Gibson, S.C. Haines, C.R. Jones, M. Kenzie and G. Lovell, *Study of the sensitivity to CKM angle γ under simultaneous determination from multiple B meson decay modes*, *Phys. Rev. D* **102** (2020) 053003 [arXiv:1909.00600] [INSPIRE].

[25] A. Bondar and A. Poluektov, *The use of quantum-correlated D^0 decays for ϕ_3 measurement*, *Eur. Phys. J. C* **55** (2008) 51 [arXiv:0801.0840] [INSPIRE].

[26] A. Bondar, A. Poluektov and V. Vorobiev, *Charm mixing in the model-independent analysis of correlated $D^0\bar{D}^0$ decays*, *Phys. Rev. D* **82** (2010) 034033 [arXiv:1004.2350] [INSPIRE].

[27] M. Bjørn and S. Malde, *CP violation and material interaction of neutral kaons in measurements of the CKM angle γ using $B^\pm \to DK^\pm$ decays where $D \to K_S^0 \pi^+ \pi^-$*, *JHEP* **07** (2019) 106 [arXiv:1904.01129] [INSPIRE].

[28] BELLE collaboration, *The Belle Detector*, *Nucl. Instrum. Meth. A* **479** (2002) 117 [INSPIRE].

[29] BELLE collaboration, *Physics Achievements from the Belle Experiment*, *PTEP* **2012** (2012) 04D001 [arXiv:1212.5342] [INSPIRE].

[30] S. Kurokawa and E. Kikutani, *Overview of the KEKB accelerators*, *Nucl. Instrum. Meth. A* **499** (2003) 1 [INSPIRE].

[31] T. Abe et al., *Achievements of KEKB*, *PTEP* **2013** (2013) 03A001 [INSPIRE].

[32] BELLE II collaboration, *Belle II Technical Design Report*, arXiv:1011.0352 [INSPIRE].

[33] SUPERKEKB collaboration, *SuperKEKB Collider*, *Nucl. Instrum. Meth. A* **907** (2018) 188 [arXiv:1809.01958] [INSPIRE].

[34] D.J. Lange, *The EvtGen particle decay simulation package*, *Nucl. Instrum. Meth. A* **462** (2001) 152 [INSPIRE].

[35] B.F.L. Ward, S. Jadach and Z. Was, *Precision calculation for $e^+e^- \to 2f$: The KK MC project*, *Nucl. Phys. B Proc. Suppl.* **116** (2003) 73 [hep-ph/0211132] [INSPIRE].

[36] T. Sjöstrand, S. Mrenna and P.Z. Skands, *A Brief Introduction to PYTHIA 8.1*, *Comput. Phys. Commun.* **178** (2008) 852 [arXiv:0710.3820] [INSPIRE].

[37] R. Brun et al., *GEANT 3.21*, CERN Program Library Long Writeup W5013, unpublished [INSPIRE].

[38] GEANT4 collaboration, *GEANT4 — a simulation toolkit*, *Nucl. Instrum. Meth. A* **506** (2003) 250 [INSPIRE].

[39] E. Barberio and Z. Was, *PHOTOS: A Universal Monte Carlo for QED radiative corrections. Version 2.0*, *Comput. Phys. Commun.* **79** (1994) 291 [INSPIRE].

[40] P.M. Lewis et al., *First Measurements of Beam Backgrounds at SuperKEKB*, *Nucl. Instrum. Meth. A* **914** (2019) 69 [arXiv:1802.01366] [INSPIRE].

[41] BELLE II FRAMEWORK SOFTWARE GROUP collaboration, *The Belle II Core Software*, *Comput. Softw. Big Sci.* **3** (2019) 1 [arXiv:1809.04299] [INSPIRE].

[42] M. Gelb et al., *B2BII: Data Conversion from Belle to Belle II*, *Comput. Softw. Big Sci.* **2** (2018) 9 [arXiv:1810.00019] [INSPIRE].

[43] BELLE collaboration, *Evidence for the Suppressed Decay $B^- \to DK^-, D^- \to K^+\pi^-$*, *Phys. Rev. Lett.* **106** (2011) 231803 [arXiv:1103.5951] [INSPIRE].

[44] BELLE II collaboration, *Study of $B \to D^{(*)}h$ decays using 62.8 fb^{-1} of Belle II data*, in *55th Rencontres de Moriond on QCD and High Energy Interactions*, (2021) [arXiv:2104.03628] [INSPIRE].

[45] H. Nakano, *Search for new physics by a time-dependent CP violation analysis of the decay $B \to K_S\eta\gamma$ using the Belle detector*, Ph.D. Thesis, Tohoku University (2014), unpublished [https://belle.kek.jp/belle/theses/doctor/nakano15.pdf].

[46] T. Keck, *FastBDT: A Speed Optimized Multivariate Classification Algoritm for the Belle II Experiment*, *Comput. Softw. Big Sci.* **1** (2017) 2 [INSPIRE].

[47] G.C. Fox and S. Wolfram, *Observables for the Analysis of Event Shapes in e^+e^- Annihilation and Other Processes*, *Phys. Rev. Lett.* **41** (1978) 1581 [INSPIRE].

[48] BELLE collaboration, *Evidence for $B^0 \to \pi^0\pi^0$*, *Phys. Rev. Lett.* **91** (2003) 261801 [hep-ex/0308040] [INSPIRE].

[49] BELLE collaboration, *Neutral B Flavor Tagging for the Measurement of Mixing-induced* CP *Violation at Belle*, *Nucl. Instrum. Meth. A* **533** (2004) 516 [hep-ex/0403022] [INSPIRE].

[50] BELLE II collaboration, *B-flavor tagging at Belle II*, arXiv:2110.00790 [INSPIRE].

[51] A. Hocker et al., *TMVA — Toolkit for Multivariate Data Analysis*, physics/0703039 [INSPIRE].

[52] W.H. Press, S.A. Teukolsky, W.T. Vetterling and B.P. Flannery, *Numerical Recipes in C++ (Second Edition)*, pp. 99–101, Cambridge University Press (2002).

[53] LHCb collaboration, *Measurement of the CKM angle γ from a combination of LHCb results*, *JHEP* **12** (2016) 087 [arXiv:1611.03076] [INSPIRE].

[54] LHCb collaboration, *Simultaneous determination of CKM angle γ and charm mixing parameters*, arXiv:2110.02350 [INSPIRE].

[55] BELLE II collaboration, *The Belle II Physics Book*, *PTEP* **2019** (2019) 123C01 [*Erratum ibid.* **2020** (2020) 029201] [arXiv:1808.10567] [INSPIRE].

The BELLE and Belle II collaborations

F. Abudinén,[32] L. Aggarwal,[72] H. Ahmed,[75] H. Aihara,[110] N. Akopov,[2] S. Al Said,[109,48]
A. Aloisio,[86,25] N. Anh Ky,[42] D.M. Asner,[4] H. Atmacan,[98] V. Aushev,[80] R. Ayad,[109] V. Babu,[94]
S. Bacher,[66] S. Baehr,[47] S. Bahinipati,[34] P. Bambade,[93] Sw. Banerjee,[101] S. Bansal,[72]
J. Baudot,[94] J. Becker,[47] P.K. Behera,[37] K. Belous,[39] J.V. Bennett,[104] F.U. Bernlochner,[96]
M. Bertemes,[40] E. Bertholet,[83] M. Bessner,[99] S. Bettarini,[89,28] F. Bianchi,[91,31] T. Bilka,[8]
D. Biswas,[101] A. Bobrov,[5,68] D. Bodrov,[64,53] G. Bonvicini,[115] J. Borah,[35] A. Bozek,[66]
M. Bračko,[102,78] P. Branchini,[30] R.A. Briere,[6] T.E. Browder,[99] A. Budano,[30] S. Bussino,[90,30]
M. Campajola,[86,25] L. Cao,[13] G. Casarosa,[89,28] C. Cecchi,[88,27] D. Červenkov,[8] P. Cheema,[108]
V. Chekelian,[57] A. Chen,[63] B.G. Cheon,[20] K. Chilikin,[53] K. Chirapatpimol,[9] H.-E. Cho,[20]
S.-J. Cho,[117] S.-K. Choi,[11] Y. Choi,[79] S. Choudhury,[43] D. Cinabro,[115] L. Corona,[89,28]
S. Cunliffe,[13] T. Czank,[112] S. Das,[56] F. Dattola,[13] E. De La Cruz-Burelo,[7] G. de Marino,[93]
S.K. Maurya,[35] G. De Nardo,[86,25] M. De Nuccio,[13] G. De Pietro,[30] R. de Sangro,[24]
M. Destefanis,[91,31] S. Dey,[83] A. De Yta-Hernandez,[7] R. Dhamija,[36] A. Di Canto,[4] Z. Doležal,[8]
I. Domínguez Jiménez,[85] T.V. Dong,[15] M. Dorigo,[32] D. Dossett,[103] S. Dubey,[99] G. Dujany,[94]
M. Eliachevitch,[96] D. Epifanov,[5,68] P. Feichtinger,[40] D. Ferlewicz,[103] T. Fillinger,[94] S. Fiore,[29]
A. Fodor,[58] F. Forti,[89,28] B.G. Fulsom,[71] A. Gabrielli,[92,32] E. Ganiev,[92,32]
M. Garcia-Hernandez,[7] V. Gaur,[114] A. Gaz,[87,26] R. Giordano,[86,25] A. Giri,[36] A. Glazov,[13]
R. Godang,[107] P. Goldenzweig,[47] B. Golob,[100,78] W. Gradl,[45] E. Graziani,[30] D. Greenwald,[82]
T. Gu,[105] Y. Guan,[98] K. Gudkova,[5,68] J. Guilliams,[104] C. Hadjivasiliou,[71] S. Halder,[81]
T. Hara,[21,18] O. Hartbrich,[99] K. Hayasaka,[67] H. Hayashii,[62] S. Hazra,[81]
I. Heredia de la Cruz,[7,12] A. Hershenhorn,[97] T. Higuchi,[112] E.C. Hill,[97] W.-S. Hou,[65]
C.-L. Hsu,[108] T. Iijima,[59,61] K. Inami,[59] A. Ishikawa,[21,18] M. Iwasaki,[69] W.W. Jacobs,[38]
E.-J. Jang,[19] Y. Jin,[32] H. Junkerkalefeld,[96] A.B. Kaliyar,[81] K.H. Kang,[112] R. Karl,[13]
G. Karyan,[2] Y. Kato,[59,61] C. Ketter,[99] C. Kiesling,[57] C.-H. Kim,[20] D.Y. Kim,[77] K.-H. Kim,[49]
Y.-K. Kim,[117] K. Kinoshita,[98] P. Kodyš,[8] T. Koga,[21] S. Kohani,[99] S. Korpar,[102,78]
E. Kovalenko,[5,68] T.M.G. Kraetzschmar,[57] P. Križan,[100,78] P. Krokovny,[5,68] T. Kuhr,[55]
J. Kumar,[6] M. Kumar,[56] R. Kumar,[73] K. Kumara,[115] A. Kuzmin,[5,68] Y.-J. Kwon,[117]
S. Lacaprara,[26] Y.-T. Lai,[112] C. La Licata,[112] L. Lanceri,[32] J.S. Lange,[46] R. Leboucher,[1]
S.C. Lee,[52] P. Leitl,[57] J. Li,[52] S.X. Li,[17] L. Li Gioi,[57] J. Libby,[37] K. Lieret,[55] Z. Liptak,[23]
Q.Y. Liu,[13] D. Liventsev,[115,21] S. Longo,[13] T. Lueck,[55] C. Lyu,[96] M. Maggiora,[91,31] R. Maiti,[40]
S. Maity,[34] R. Manfredi,[92,32] E. Manoni,[27] S. Marcello,[91,31] A. Martini,[13] L. Massaccesi,[89,28]
M. Masuda,[111,70] K. Matsuoka,[21] D. Matvienko,[5,53,68] J.A. McKenna,[97] F. Meier,[14]
M. Merola,[86,25] F. Metzner,[47] M. Milesi,[103] C. Miller,[113] K. Miyabayashi,[62] R. Mizuk,[53,64]
G.B. Mohanty,[81] N. Molina-Gonzalez,[7] H.-G. Moser,[57] F. Mueller,[57] C. Murphy,[112] R. Mussa,[31]
K.R. Nakamura,[21,18] T. Nakano,[70] M. Nakao,[21,18] M. Naruki,[51] D. Narwal,[35] A. Natochii,[99]
L. Nayak,[36] M. Nayak,[83] G. Nazaryan,[2] N.K. Nisar,[4] S. Nishida,[21,18] K. Nishimura,[99]
Y. Onishchuk,[80] H. Ono,[67] P. Oskin,[53] G. Pakhlova,[64,53] A. Paladino,[89,28] A. Panta,[104]
E. Paoloni,[89,28] K. Parham,[14] S.-H. Park,[21] A. Passeri,[30] A. Pathak,[101] S. Patra,[33]
R. Pestotnik,[78] L.E. Piilonen,[114] T. Podobnik,[78] S. Pokharel,[104] L. Polat,[1] C. Praz,[13]
S. Prell,[43] E. Prencipe,[46] M.T. Prim,[96] H. Purwar,[99] A. Rabusov,[82] P. Rados,[40] S. Raiz,[92,32]
S. Reiter,[46] M. Remnev,[5,68] I. Ripp-Baudot,[94] G. Rizzo,[89,28] L.B. Rizzuto,[78]
S.H. Robertson,[58,41] M. Röhrken,[13] J.M. Roney,[113,41] A. Rostomyan,[13] N. Rout,[37] D. Sahoo,[43]
D.A. Sanders,[104] S. Sandilya,[36] L. Santelj,[100,78] Y. Sato,[21] V. Savinov,[105] B. Scavino,[45]
G. Schnell,[95,3] J. Schueler,[99] A.J. Schwartz,[98] Y. Seino,[67] A. Selce,[30,16] K. Senyo,[116]
M.E. Sevior,[103] M. Shapkin,[39] C. Sharma,[56] T. Shillington,[58] B. Shwartz,[5,68] A. Sibidanov,[99]
F. Simon,[57] J.B. Singh,[72,a] A. Soffer,[83] E. Solovieva,[53] S. Spataro,[91,31] B. Spruck,[45]

S. Stefkova,[13] Z.S. Stottler,[114] R. Stroili,[87,26] K. Sumisawa,[21,18] W. Sutcliffe,[96] S.Y. Suzuki,[21,18]
M. Tabata,[10] M. Takizawa,[74,22,76] K. Tanida,[44] F. Tenchini,[89,28] R. Tiwary,[81] D. Tonelli,[32]
E. Torassa,[26] K. Trabelsi,[93] M. Uchida,[84] I. Ueda,[21,18] T. Uglov,[53,64] K. Uno,[67] S. Uno,[21,18]
Y. Ushiroda,[21,18,110] S.E. Vahsen,[99] R. van Tonder,[96] K.E. Varvell,[108] A. Vinokurova,[5,68]
L. Vitale,[92,32] H.M. Wakeling,[58] E. Wang,[105] M.-Z. Wang,[65] X.L. Wang,[17] A. Warburton,[58]
S. Watanuki,[117] O. Werbycka,[66] C. Wessel,[96] E. Won,[50] B.D. Yabsley,[108] W. Yan,[106] H. Ye,[13]
K. Yoshihara,[59] Y. Yusa,[67] L. Zani,[1] Y. Zhai,[43] Y. Zhang,[17] V. Zhilich,[5,68] Q.D. Zhou,[59,60,61]
X.Y. Zhou,[54] V.I. Zhukova,[53]

[1] *Aix Marseille Université, CNRS/IN2P3, CPPM, 13288 Marseille, France*
[2] *Alikhanyan National Science Laboratory, Yerevan 0036, Armenia*
[3] *IKERBASQUE, Basque Foundation for Science, 48013 Bilbao, Spain*
[4] *Brookhaven National Laboratory, Upton, New York 11973, U.S.A.*
[5] *Budker Institute of Nuclear Physics SB RAS, Novosibirsk 630090, Russian Federation*
[6] *Carnegie Mellon University, Pittsburgh, Pennsylvania 15213, U.S.A.*
[7] *Centro de Investigacion y de Estudios Avanzados del Instituto Politecnico Nacional, Mexico City 07360, Mexico*
[8] *Faculty of Mathematics and Physics, Charles University, 121 16 Prague, Czech Republic*
[9] *Chiang Mai University, Chiang Mai 50202, Thailand*
[10] *Chiba University, Chiba 263-8522, Japan*
[11] *Chung-Ang University, Seoul 06974, South Korea*
[12] *Consejo Nacional de Ciencia y Tecnología, Mexico City 03940, Mexico*
[13] *Deutsches Elektronen-Synchrotron, 22607 Hamburg, Germany*
[14] *Duke University, Durham, North Carolina 27708, U.S.A.*
[15] *Institute of Theoretical and Applied Research (ITAR), Duy Tan University, Hanoi 100000, Vietnam*
[16] *ENEA Casaccia, I-00123 Roma, Italy*
[17] *Key Laboratory of Nuclear Physics and Ion-beam Application (MOE) and Institute of Modern Physics, Fudan University, Shanghai 200443, China*
[18] *The Graduate University for Advanced Studies (SOKENDAI), Hayama 240-0193, Japan*
[19] *Gyeongsang National University, Jinju 52828, South Korea*
[20] *Department of Physics and Institute of Natural Sciences, Hanyang University, Seoul 04763, South Korea*
[21] *High Energy Accelerator Research Organization (KEK), Tsukuba 305-0801, Japan*
[22] *J-PARC Branch, KEK Theory Center, High Energy Accelerator Research Organization (KEK), Tsukuba 305-0801, Japan*
[23] *Hiroshima University, Higashi-Hiroshima, Hiroshima 739-8530, Japan*
[24] *INFN Laboratori Nazionali di Frascati, I-00044 Frascati, Italy*
[25] *INFN Sezione di Napoli, I-80126 Napoli, Italy*
[26] *INFN Sezione di Padova, I-35131 Padova, Italy*
[27] *INFN Sezione di Perugia, I-06123 Perugia, Italy*
[28] *INFN Sezione di Pisa, I-56127 Pisa, Italy*
[29] *INFN Sezione di Roma, I-00185 Roma, Italy*
[30] *INFN Sezione di Roma Tre, I-00146 Roma, Italy*
[31] *INFN Sezione di Torino, I-10125 Torino, Italy*
[32] *INFN Sezione di Trieste, I-34127 Trieste, Italy*
[33] *Indian Institute of Science Education and Research Mohali, SAS Nagar, 140306, India*
[34] *Indian Institute of Technology Bhubaneswar, Satya Nagar 751007, India*
[35] *Indian Institute of Technology Guwahati, Assam 781039, India*
[36] *Indian Institute of Technology Hyderabad, Telangana 502285, India*
[37] *Indian Institute of Technology Madras, Chennai 600036, India*
[38] *Indiana University, Bloomington, Indiana 47408, U.S.A.*
[39] *Institute for High Energy Physics, Protvino 142281, Russian Federation*

40 Institute of High Energy Physics, Vienna 1050, Austria

41 Institute of Particle Physics (Canada), Victoria, British Columbia V8W 2Y2, Canada

42 Institute of Physics, Vietnam Academy of Science and Technology (VAST), Hanoi, Vietnam

43 Iowa State University, Ames, Iowa 50011, U.S.A.

44 Advanced Science Research Center, Japan Atomic Energy Agency, Naka 319-1195, Japan

45 Institut für Kernphysik, Johannes Gutenberg-Universität Mainz, D-55099 Mainz, Germany

46 Justus-Liebig-Universität Gießen, 35392 Gießen, Germany

47 Institut für Experimentelle Teilchenphysik, Karlsruher Institut für Technologie, 76131 Karlsruhe, Germany

48 Department of Physics, Faculty of Science, King Abdulaziz University, Jeddah 21589, Saudi Arabia

49 Korea Institute of Science and Technology Information, Daejeon 34141, South Korea

50 Korea University, Seoul 02841, South Korea

51 Kyoto University, Kyoto 606-8501, Japan

52 Kyungpook National University, Daegu 41566, South Korea

53 P.N. Lebedev Physical Institute of the Russian Academy of Sciences, Moscow 119991, Russian Federation

54 Liaoning Normal University, Dalian 116029, China

55 Ludwig Maximilians University, 80539 Munich, Germany

56 Malaviya National Institute of Technology Jaipur, Jaipur 302017, India

57 Max-Planck-Institut für Physik, 80805 München, Germany

58 McGill University, Montréal, Québec, H3A 2T8, Canada

59 Graduate School of Science, Nagoya University, Nagoya 464-8602, Japan

60 Institute for Advanced Research, Nagoya University, Nagoya 464-8602, Japan

61 Kobayashi-Maskawa Institute, Nagoya University, Nagoya 464-8602, Japan

62 Nara Women's University, Nara 630-8506, Japan

63 National Central University, Chung-li 32054, Taiwan

64 National Research University Higher School of Economics, Moscow 101000, Russian Federation

65 Department of Physics, National Taiwan University, Taipei 10617, Taiwan

66 H. Niewodniczanski Institute of Nuclear Physics, Krakow 31-342, Poland

67 Niigata University, Niigata 950-2181, Japan

68 Novosibirsk State University, Novosibirsk 630090, Russian Federation

69 Osaka City University, Osaka 558-8585, Japan

70 Research Center for Nuclear Physics, Osaka University, Osaka 567-0047, Japan

71 Pacific Northwest National Laboratory, Richland, Washington 99352, U.S.A.

72 Panjab University, Chandigarh 160014, India

73 Punjab Agricultural University, Ludhiana 141004, India

74 Meson Science Laboratory, Cluster for Pioneering Research, RIKEN, Saitama 351-0198, Japan

75 St. Francis Xavier University, Antigonish, Nova Scotia, B2G 2W5, Canada

76 Showa Pharmaceutical University, Tokyo 194-8543, Japan

77 Soongsil University, Seoul 06978, South Korea

78 J. Stefan Institute, 1000 Ljubljana, Slovenia

79 Sungkyunkwan University, Suwon 16419, South Korea

80 Taras Shevchenko National Univ. of Kiev, Kiev, Ukraine

81 Tata Institute of Fundamental Research, Mumbai 400005, India

82 Department of Physics, Technische Universität München, 85748 Garching, Germany

83 Tel Aviv University, School of Physics and Astronomy, Tel Aviv, 69978, Israel

84 Tokyo Institute of Technology, Tokyo 152-8550, Japan

85 Universidad Autonoma de Sinaloa, Sinaloa 80000, Mexico

86 Dipartimento di Scienze Fisiche, Università di Napoli Federico II, I-80126 Napoli, Italy

87 Dipartimento di Fisica e Astronomia, Università di Padova, I-35131 Padova, Italy

88 Dipartimento di Fisica, Università di Perugia, I-06123 Perugia, Italy

89 Dipartimento di Fisica, Università di Pisa, I-56127 Pisa, Italy

90 *Dipartimento di Matematica e Fisica, Università di Roma Tre, I-00146 Roma, Italy*

91 *Dipartimento di Fisica, Università di Torino, I-10125 Torino, Italy*

92 *Dipartimento di Fisica, Università di Trieste, I-34127 Trieste, Italy*

93 *Université Paris-Saclay, CNRS/IN2P3, IJCLab, 91405 Orsay, France*

94 *Université de Strasbourg, CNRS, IPHC, UMR 7178, 67037 Strasbourg, France*

95 *Department of Physics, University of the Basque Country UPV/EHU, 48080 Bilbao, Spain*

96 *University of Bonn, 53115 Bonn, Germany*

97 *University of British Columbia, Vancouver, British Columbia, V6T 1Z1, Canada*

98 *University of Cincinnati, Cincinnati, Ohio 45221, U.S.A.*

99 *University of Hawaii, Honolulu, Hawaii 96822, U.S.A.*

100 *Faculty of Mathematics and Physics, University of Ljubljana, 1000 Ljubljana, Slovenia*

101 *University of Louisville, Louisville, Kentucky 40292, U.S.A.*

102 *Faculty of Chemistry and Chemical Engineering, University of Maribor, 2000 Maribor, Slovenia*

103 *School of Physics, University of Melbourne, Victoria 3010, Australia*

104 *University of Mississippi, University, Mississippi 38677, U.S.A.*

105 *University of Pittsburgh, Pittsburgh, Pennsylvania 15260, U.S.A.*

106 *University of Science and Technology of China, Hefei 230026, China*

107 *University of South Alabama, Mobile, Alabama 36688, U.S.A.*

108 *School of Physics, University of Sydney, New South Wales 2006, Australia*

109 *Department of Physics, Faculty of Science, University of Tabuk, Tabuk 71451, Saudi Arabia*

110 *Department of Physics, University of Tokyo, Tokyo 113-0033, Japan*

111 *Earthquake Research Institute, University of Tokyo, Tokyo 113-0032, Japan*

112 *Kavli Institute for the Physics and Mathematics of the Universe (WPI), University of Tokyo, Kashiwa 277-8583, Japan*

113 *University of Victoria, Victoria, British Columbia, V8W 3P6, Canada*

114 *Virginia Polytechnic Institute and State University, Blacksburg, Virginia 24061, U.S.A.*

115 *Wayne State University, Detroit, Michigan 48202, U.S.A.*

116 *Yamagata University, Yamagata 990-8560, Japan*

117 *Yonsei University, Seoul 03722, South Korea*

[a] *Also at University of Petroleum and Energy Studies, Dehradun 248007, India*